Cholinergic interneuron inhibition potentiates corticostriatal transmission in direct medium spiny neurons and rescues motor learning in parkinsonism

Gwenaëlle Laverne, Jonathan Pesce, Ana Reynders, Etienne Combrisson, Eduardo Gascon, Christophe Melon, Lydia Kerkerian-Le Goff, Nicolas Maurice, Corinne Beurrier

Cell Reports

Article

Cholinergic interneuron inhibition potentiates corticostriatal transmission in direct medium spiny neurons and rescues motor learning in parkinsonism

Graphical abstract

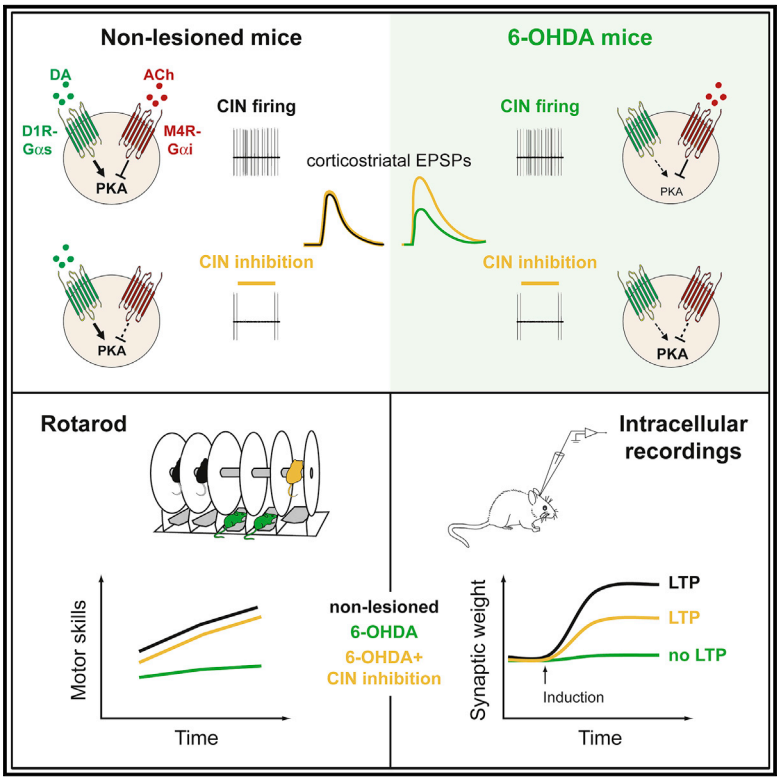

Authors

Gwenaëlle Laverne, Jonathan Pesce, Ana Reynders, ..., Lydia Kerkerian-Le Goff, Nicolas Maurice, Corinne Beurrier

Correspondence

corinne.beurrier@univ-amu.fr

In brief

Laverne et al. show that in parkinsonian mice, opto-inhibition of striatal cholinergic interneurons (CINs) in slices potentiates corticostriatal transmission in D1 MSNs via M4 mAChR and PKA. *In vivo*, it induces a partial rescue of corticostriatal LTP and motor learning. These findings make CINs potential therapeutic targets in Parkinson's disease.

Highlights

- CIN inhibition potentiates corticostriatal transmission in D1 MSNs in parkinsonian state
- This is due to disruption of a PKA-dependent signaling pathway linked to M4 mAChR
- CIN inhibition partially recues corticostriatal LTP in MSNs in parkinsonian mice
- CIN inhibition improves motor skill learning in parkinsonian mice

Laverne et al., 2022, Cell Reports *40*, 111034
July 5, 2022
https://doi.org/10.1016/j.celrep.2022.111034

CellPress

Cell Reports

CellPress
OPEN ACCESS

Article

Cholinergic interneuron inhibition potentiates corticostriatal transmission in direct medium spiny neurons and rescues motor learning in parkinsonism

Gwenaëlle Laverne,[1] Jonathan Pesce,[1] Ana Reynders,[1] Etienne Combrisson,[2] Eduardo Gascon,[2] Christophe Melon,[1] Lydia Kerkerian-Le Goff,[1] Nicolas Maurice,[1,3,4] and Corinne Beurrier[1,3,4,5,*]

[1]Aix Marseille University, CNRS, Institut de Biologie du Développement (IBDM), 13009 Marseille, France
[2]Aix Marseille University, CNRS, Institut de Neurosciences de la Timone (INT), 13005 Marseille, France
[3]Present address: Aix Marseille University, CNRS, Institut de Neurosciences de la Timone (INT), 13005 Marseille, France
[4]These authors contributed equally
[5]Lead contact
*Correspondence: corinne.beurrier@univ-amu.fr
https://doi.org/10.1016/j.celrep.2022.111034

SUMMARY

Striatal cholinergic interneurons (CINs) respond to salient or reward prediction-related stimuli after conditioning with brief pauses in their activity, implicating them in learning and action selection. This pause is lost in animal models of Parkinson's disease. How this signal regulates the striatal network remains an open question. Here, we examine the impact of CIN firing inhibition on glutamatergic transmission between the cortex and the medium spiny neurons expressing dopamine D1 receptor (D1 MSNs). Brief interruption of CIN activity has no effect in control conditions, whereas it increases glutamatergic responses in D1 MSNs after dopamine denervation. This potentiation depends upon M4 muscarinic receptor and protein kinase A. Decreasing CIN firing by optogenetics/chemogenetics *in vivo* partially rescues long-term potentiation in MSNs and motor learning deficits in parkinsonian mice. Our findings demonstrate that the control exerted by CINs on corticostriatal transmission and striatal-dependent motor-skill learning depends on the integrity of dopaminergic inputs.

INTRODUCTION

Voluntary movement and action planning depend on the balanced activity of two distinct populations of GABAergic projection neurons in the striatum called medium-sized spiny neurons (MSNs). MSNs expressing D1 dopamine (DA) receptor (D1 MSNs) project to the basal ganglia output nuclei, forming the so-called direct pathway, whereas MSNs expressing D2 receptor (D2 MSNs) primarily project to the globus pallidus, forming the first link of the indirect pathway (Albin et al., 1989; DeLong, 1990). MSN firing relies on excitatory inputs from the cerebral cortex and the thalamus and is modulated by DA afferents from the substantia nigra pars compacta (SNc). DA is expected to induce motor activation by simultaneously activating D1 MSNs to promote selected actions and depressing D2 MSNs to suppress competing actions. In Parkinson's disease (PD), the loss of nigrostriatal DA neurons results in an imbalance in favor of the indirect pathway, the activities of D1 MSNs and D2 MSNs being inappropriately decreased and increased, respectively (DeLong, 1990; Mallet et al., 2005; Smith et al., 1998). These cell-specific changes are thought to underlie most parkinsonian motor deficits, including akinesia.

In addition to DA, the striatum exhibits a rich cholinergic innervation and expresses high levels of acetylcholine (ACh), muscarinic receptors (mAChRs) and other markers related to ACh. mAChRs are distributed on the two populations of MSNs, on interneurons, and on synaptic terminals, including glutamatergic axons (Goldberg et al., 2012). At the post-synaptic level, the Gαq-coupled M1 mAChR is present on both D1 and D2 MSNs while the Gαi-coupled M4 mAChR is preferentially expressed by D1 MSNs (Hersch et al., 1994; Yan et al., 2001). The effects of mAChR activation have been mostly investigated using the application of exogenous agonists in conjunction with whole-cell patch-clamp recording *ex vivo*. This approach has revealed a variety of effects on MSN intrinsic excitability and excitatory synaptic transmission, depending on the type of mAChR targeted (Abudukeyoumu et al., 2019; Hernández-Flores et al., 2015; Zhai et al., 2018). However, sustained application of specific receptor agonists does not recapitulate the spatiotemporal dynamics of endogenous ACh.

In the striatum, cholinergic interneurons (CINs) are the main source of ACh. Despite their small number (1%–2% of striatal cells), CINs harbor dense terminal fields that contact both populations of MSNs and are therefore well positioned to regulate striatal outflow. In monkeys, tonically active neurons (TANs), which are likely CINs, transiently respond to motivationally relevant events with a brief pause in their tonic firing and are, for this reason, considered key players in learning and decision making

(Aosaki et al., 1994a; Apicella et al., 1992; Goldberg and Reynolds, 2011). The pause is mostly synchronized in the TAN population such as it may efficiently translate into global reduction of the striatal ACh level (Aosaki et al., 1995). In PD, these neurons lose their ability to pause and inhibition of their discharge using optogenetic or chemogenetic tools improves motor performances in mouse models of PD (Aosaki et al., 1994b; Maurice et al., 2015; Tanimura et al., 2019; Ztaou et al., 2016). A normalization of D2 MSN activity via their thalamic inputs may in part underlie this beneficial effect (Tanimura et al., 2019). However, we have shown that CIN opto-inhibition in parkinsonian mice had a selective impact on the component of the complex cortically evoked neuronal responses in the substantia nigra pars reticulata mediated by the direct pathway (Maurice et al., 2015). This suggests that CINs also act on the trans-striatal processing of cortical information through D1 MSNs. However, how a synchronous inhibition of CIN activity shapes the dynamics of corticostriatal processing in these neurons in control and PD conditions remains largely unexplored. To fill this gap, we used the optogenetic inhibition of CIN firing in conjunction with recordings of synaptic responses triggered by cortical stimulation in genetically identified D1 MSNs in mouse striatal slices. After showing that inhibition of CIN firing triggered a potentiation of corticostriatal transmission in D1 MSNs in parkinsonian mice, but not in non-lesioned mice, we further explored the mechanisms underlying this effect. We also investigated whether optogenetic and chemogenetic inhibition of CINs *in vivo* could interfere with alterations in long-term potentiation (LTP) at corticostriatal synapses and motor learning in parkinsonian conditions. Our results demonstrate that in the parkinsonian state, the control exerted by CINs on corticostriatal transmission is altered in D1 MSNs via M4 mAChR-mediated mechanisms. Abnormal signaling by CINs also contributes to dysfunctional long-term plasticity at corticostriatal synapses and to disease symptoms.

RESULTS

All of the mice used in this study were 2–4 months old at the time of the experiments. The extent of the DA lesion was assessed by quantitative analysis of tyrosine hydroxylase (TH) immunostaining in the striatum, except for the experimental groups with intrastriatal injection of adeno-associated virus (AAV) in which TH was quantified in the SNc. All parkinsonian mice used in this study had DA depletion $\geq$70% (Figure S1A). Summary statistics (median and interquartile range, means, and SEM), associated numbers of cells and mice, and p values for each statistical comparison are shown for all of the datasets in the tables in the supplemental information.

Opto-inhibition of CINs induces a potentiation of corticostriatal synaptic transmission in D1 MSNs from 6-hydroxydopamine (6-OHDA) mice

Immunohistochemical labeling experiments showed that halorhodopsin (eNpHR) exclusively overlaps with choline acetyltransferase (ChAT)-expressing neurons in the striatum of ChAT$^{cre/wt}$; Rosa$^{NpHR/wt}$ transgenic mice (Figure S1B). In *in vitro* brain slices, the application of brief light stimulation (150 ms at 585 nm) induced a complete and reliable inhibition of the firing of eNpHR-enhanced yellow fluorescent protein (EYFP)-expressing CINs (Figures S1C–S1E). To determine whether such inhibition modulates corticostriatal synaptic transmission in control and PD-like conditions, we recorded excitatory post-synaptic potentials (EPSPs) evoked by the electrical stimulation of cortical fibers in D1 MSNs identified by tdTomato expression in triple-transgenic ChAT$^{cre/wt}$; Rosa$^{NpHR/wt}$; D1-tdTomato$^{+/-}$ mice (see Method details) (Figure 1A). We found that the amplitude of the EPSPs, as well as the paired-pulse ratio (PPR, 50 ms interstimulus interval), were not significantly altered by CIN opto-inhibition in non-lesioned mice (Figures 1B; Table S1). These parameters were also not modified when CIN opto-inhibition was performed in the presence of neostigmine (Figure S2A; Table S1), an inhibitor of acetylcholinesterase known to increase extracellular ACh, which per se decreased EPSP amplitude and increased PPR (Figure S2B). Therefore, the lack of modulation of EPSP amplitude by CIN opto-inhibition was not due to insufficient cholinergic tone in slices. Consistently, opto-inhibition of CINs performed in anesthetized mice in which ACh tone is not altered by the slicing procedure did not affect the cortically evoked EPSPs (Figure S3; Table S1). In sharp contrast, CIN opto-inhibition significantly increased EPSP amplitude in D1 MSNs from 6-OHDA mice without affecting PPR (Figure 1C; Table S1). Between-group comparison showed that EPSP potentiation was specific to 6-OHDA mice (Table S1). This potentiation was not observed in D1 MSNs recorded from littermate 6-OHDA mice that do not express Cre recombinase in cholinergic neurons, excluding non-specific light-induced effects (Figure S4; Table S1). Together, these findings show that a brief interruption of CIN firing potentiates corticostriatal synaptic transmission in D1 MSNs after striatal DA denervation, suggesting that abnormal cholinergic signaling affects corticostriatal information processing through the direct pathway in PD-like condition.

Interruption of a signaling pathway involving M4 mAChR and protein kinase A (PKA) mediates the effect of CIN opto-inhibition on corticostriatal transmission

The finding that CIN opto-inhibition enhances cortically evoked EPSPs in D1 MSNs in 6-OHDA mice without modifying PPR suggests a post-synaptic locus of action. We therefore tested whether M4 mAChR, which is preferentially expressed by D1 MSNs, is involved in this effect. In this case, M4 mAChR pharmacological blockade should not only potentiate corticostriatal transmission, as does CIN opto-inhibition, but also occlude the effect of CIN opto-inhibition. Bath application of tropicamide (1 μM) produced a marked increase in EPSP amplitude (at 22 min, +61% $\pm$ 0.23% of baseline, n = 5) without affecting PPR (Figure 2A). Under tropicamide, CIN opto-inhibition failed to affect corticostriatal EPSPs (Figures 2B and 2D; Table S1). Activation of Gαi-coupled M4 mAChR inhibits PKA activity. Therefore, CINs may affect corticostriatal transmission through post-synaptic modulation of PKA. To test this hypothesis, the membrane impermeable non-myristoylated form of PKA inhibitor (PKI 6–22 amide, 20 μM) was delivered into D1 MSNs via the recording pipette. In this condition, EPSP amplitude remained unchanged from baseline levels during CIN opto-inhibition (Figures 2C and 2D; Table S1). Because these results strongly

Please cite this article in press as: Laverne et al., Cholinergic interneuron inhibition potentiates corticostriatal transmission in direct medium spiny neurons and rescues motor learning in parkinsonism, Cell Reports (2022), https://doi.org/10.1016/j.celrep.2022.111034

CellPress
OPEN ACCESS

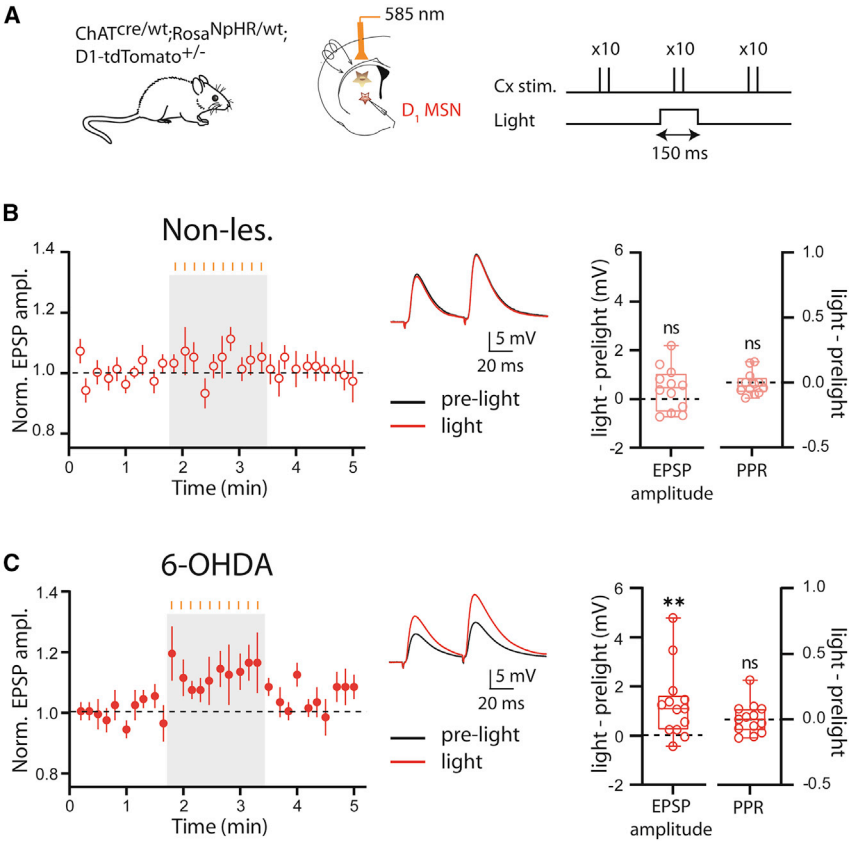

Figure 1. Corticostriatal EPSPs in D1 MSNs are increased by CIN opto-inhibition in 6-OHDA mice

(A) Schematic of the experimental approach.

(B and C) Time courses (means ± SEMs) of normalized EPSP amplitude recorded in non-lesioned (B, n = 12) and 6-OHDA (C, n = 13) mice before, during, and after CIN opto-inhibition. Light delivery (10 pulses, 150-ms width at 1 Hz) is indicated by the orange vertical bars above the gray rectangle. Representative example of averaged EPSP traces (10 consecutive trials) recorded in non-lesioned (B) and 6-OHDA (C) mice before (pre-light) and during (light) opto-inhibition of CINs. Paired cortical stimulations (50 ms interval) were delivered every 10 s. Box-and-whisker plots illustrate the difference in EPSP amplitude and PPR evoked in light versus pre-light conditions and indicate median, first and third quartiles, minimum and maximum values. **p < 0.01; ns, not significant.

See Table S1 for statistical information.

argue for a critical involvement of M4 mAChR in D1 MSNs, we next measured by qRT-PCR the relative abundance of *Chrma4* mRNAs encoding for M4 mAChR subunits in fluorescence-activated cell sorting (FACS)-sorted D1 MSNs from Drd1a-tdTomato mice, 28–33 days post-vehicle or 6-OHDA injection. Taking *Gapdh* as a reference gene because its expression was not affected by the 6-OHDA lesion (data not shown), the results showed no significant difference between the two conditions (Figures 2E; Table S1). We next determined the functional impact of M4 mAChR activation by endogenous ACh using an electrophysiological readout of M4 mAChR activation. For that, we virally expressed G protein-activated potassium channels (GIRK2) in MSNs that do not express this channel endogenously, by injecting an AAV encoding tdTomato and GIRK2 into the dorsal striatum (Mamaligas and Ford, 2016). Western blot analysis, performed 26–30 days after AAV-GIRK2 injection, confirmed that these injections led to an overexpression of GIRK2 compared with the endogenous level in the striatum of non-injected mice (data not shown). More important, GIRK2 overexpression was not affected by DA depletion (Figure S5B). Application of the muscarinic agonist carbachol (10 μM) evoked an outward current in a portion of tdTomato+ MSNs (Figure S5C). In the absence of mAChR stimulation, 33% of tdTomato+ MSNs exhibited spontaneous inhibitory post-synaptic currents (sIPSCs) that were suppressed by tropicamide (1 μM, n = 3), a preferential antagonist of M4 mAChR (Figure S5D). These results showed that GIRK2 channels efficiently couple to Gαi-linked M4 mAChR in a fraction of tdTomato+ MSNs that are likely D1 MSNs, as previously reported (Mamaligas and Ford, 2016). We then compared the frequency and the amplitude of sIPSCs recorded in non-lesioned and 6-OHDA mice and found no significant difference between the two groups (Figure 2F; Table S1). Overall, these results indicate that, in D1 MSNs, the DA lesion disrupts a PKA-dependent signaling pathway linked to M4 mAChR, but it does not dramatically alter their expression level and sensitivity to endogenous ACh.

Corticostriatal LTP is lost *in vivo* in parkinsonian mice and is partially restored by CIN opto-inhibition

Slice experiments have provided compelling evidence for altered long-term plasticity at corticostriatal synapses in PD conditions. Whether this also occurs *in vivo* after chronic DA depletion and is related to CIN activity remains an open question. To address this issue, we used a protocol efficient to induce LTP *in vivo* in non-lesioned mice, as described in a previous work in rats (Charpier and Deniau, 1997), and determined whether this form of plasticity is maintained in 6-OHDA mice. Intracellular recordings of MSNs were performed in the dorsolateral region of the striatum receiving direct inputs from the sensorimotor cortex. MSNs recorded under ketamine-xylazine anesthesia exhibited spontaneous membrane fluctuations consisting of recurrent sustained depolarization (up states) interrupted by hyperpolarizing periods (down states) (Figure 3A). EPSPs were triggered by electrical stimulation of the sensorimotor cortex during the down state to minimize EPSP amplitude fluctuations due to the different level of membrane polarization. To induce LTP, we applied 4 trains of 1-s cortical stimulation at 100 Hz at 10-s intervals coupled to the membrane depolarization of MSNs (Figure 3A). In experiments in which CIN opto-inhibition was coupled to the pairing protocol, light was applied for 1 s at the same time as the trains. As a prerequisite, we verified that CIN firing was reliably inhibited

Please cite this article in press as: Laverne et al., Cholinergic interneuron inhibition potentiates corticostriatal transmission in direct medium spiny neurons and rescues motor learning in parkinsonism, Cell Reports (2022), https://doi.org/10.1016/j.celrep.2022.111034

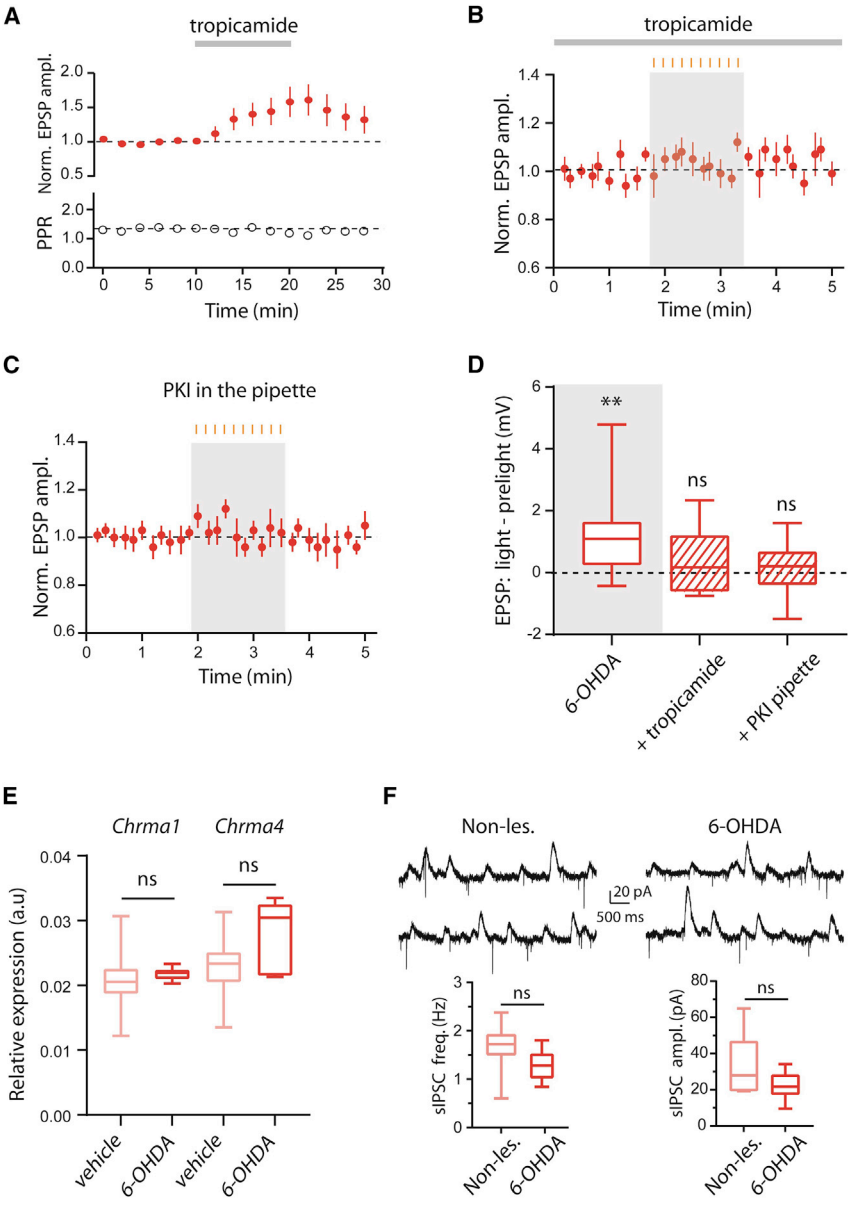

Figure 2. M4 mAChR and protein kinase A (PKA) mediate the increase in corticostriatal EPSPs induced by CIN opto-inhibition in D1 MSNs in 6-OHDA mice

(A) Normalized EPSP amplitude (means ± SEMs) as a function of time in D1 MSNs from 6-OHDA mice. Ten-minute bath application of tropicamide (1 μM) increased EPSP amplitude without affecting PPR (n = 5).

(B and C) Graphs showing normalized EPSP amplitude (means ± SEMs) as a function of time in D1 MSNs from 6-OHDA mice. CIN opto-inhibition was performed in the presence of tropicamide (1 μM, n = 10, B) and the membraneimpermeable non-myristoylated form of PKA inhibitor (PKI 6–22 amide) administered into D1 MSNs via the recording pipette (20 μM, n = 10, C). Light delivery (10 pulses, 150-ms width at 1 Hz) is indicated by the orange vertical bars above the gray rectangle.

(D) Box-and-whisker plots illustrate the effects of CIN opto-inhibition on EPSP amplitude in the presence of several pharmacological compounds. For comparison purposes, the effect of CIN opto-inhibition in D1 MSNs from 6-OHDA mice described in Figure 1C is also illustrated (gray rectangle).

(E) Relative expression of *Chrma1* and *Chrma4* mRNA, encoding, respectively, for M1 and M4 mAChR subunits, in D1 MSNs that were FACS-sorted in vehicle (n = 7) and 6-OHDA (n = 7) mice.

(F) Representative trace of sIPSCs recorded in tdTomato+ MSNs (Vh = −60 mV) from non-lesioned and 6-OHDA mice. Box-and-whisker plots show the frequency and amplitude of sIPSCs in non-lesioned (n = 7) and 6-OHDA (n = 10) mice and indicate median, first and third quartiles, minimum and maximum values. **p < 0.01; ns, not significant.

See also Table S1 for statistical information.

for the duration of the illumination (Figure 3B). On average, the EPSP slope recorded in the MSNs of non-lesioned mice was significantly increased after the pairing protocol (145.8% ± 10.6% of baseline, 20–30 min post-pairing, n = 6) (Figure 3C; Table S2). In 6-OHDA mice, the pairing protocol no longer triggered LTP (102.3% ± 3.0% of baseline, 20–30 min post-pairing, n = 5). When the same protocol was applied in 6-OHDA mice in conjunction with the opto-inhibition of CINs, it induced a significant LTP (123.8% ± 7.4% of baseline, 20–30 min post-pairing, n = 5). Intergroup comparison showed that the 6-OHDA group was significantly different from the non-lesioned group, whereas the 6-OHDA + CIN inhibition group was not, suggesting that the opto-inhibition of CINs induced a partial recovery of LTP in the parkinsonian state (Figure 3D; Table S2).

Decreasing CIN activity improves motor-skill learning in parkinsonian mice

Altered transmission and plasticity at corticostriatal synapses are considered key substrates of motor deficits and motor learning impairment in the PD state. Because CIN silencing increases corticostriatal transmission onto D1 MSNs, which are hypoactive in the PD state, and restores LTP in some MSNs, we hypothesized that the silencing of these interneurons may improve motor-skill learning in parkinsonian mice. To test this assumption, we used a chemogenetic approach, more adapted for durable modulation of neuronal activity compatible with behavioral testing. An inhibitory designer receptor exclusively activated by designer drugs (DREADD) was selectively expressed in CINs by injecting a Cre-inducible AAV carrying the gene encoding hM4Di fused to mCherry into the striatum of ChAT Cre mice. The kinetic profile of clozapine-*N*-oxide (CNO)-mediated modulation of CIN activity was determined *in vivo* by performing CIN extracellular recordings in anesthetized hM4Di-injected mice (Figure 4A). Putative CINs were identified by their typical tonic discharge

Please cite this article in press as: Laverne et al., Cholinergic interneuron inhibition potentiates corticostriatal transmission in direct medium spiny neurons and rescues motor learning in parkinsonism, Cell Reports (2022), https://doi.org/10.1016/j.celrep.2022.111034

CellPress
OPEN ACCESS

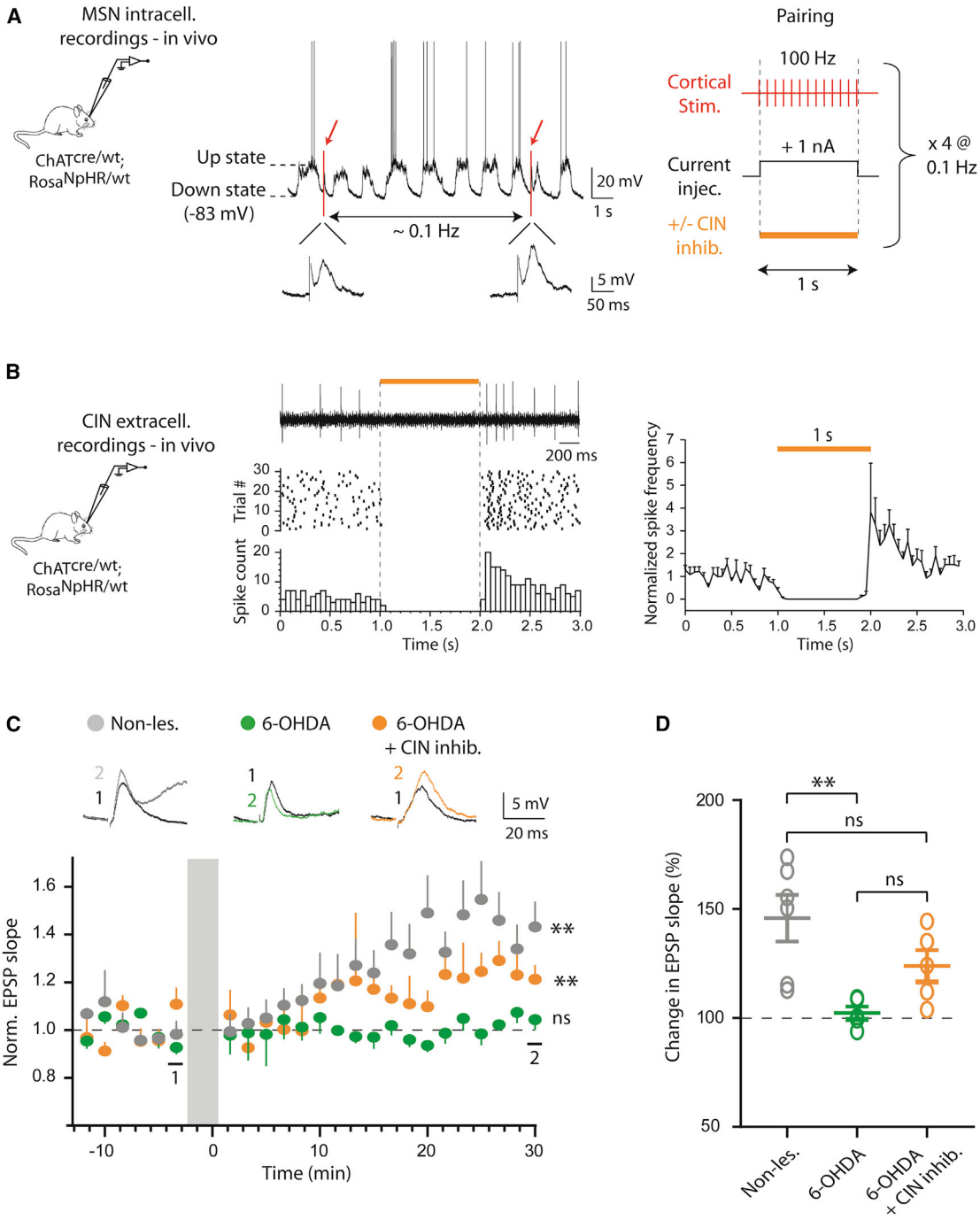

Figure 3. Corticostriatal long-term potentiation *in vivo* is partially restored by CIN opto-inhibition in parkinsonian mice

(A) Example trace of an intracellular recording from one MSN exhibiting up and down membrane fluctuations. Red arrows indicate the time when cortical stimulations were applied during the down states. Expanded traces show two cortically-evoked EPSPs. Schematic of the experimental protocol used to induce LTP: cortical tetanic stimulation (1 s at 100 Hz applied 4 times at 10-s intervals) coupled to post-synaptic membrane depolarization (+1 nA). The orange bar represents light application during the pairing protocol.

(B) Left, raster and peristimulus time histogram (PSTH) obtained in one eNpHR-expressing CIN recorded extracellularly *in vivo* in anesthetized mice showing the effect of 1-s-duration pulses of 585 nm light. Right, normalized firing frequency (means ± SEMs) of eNpHR-expressing CINs before, during, and after 1-s light application (n = 7).

(C) Time courses (means ± SEMs) of normalized EPSP slope from MSNs recorded in non-lesioned (n = 6), 6-OHDA (n = 5), and 6-OHDA + CIN opto-inhibition (n = 5) conditions before and after the pairing protocol. No recording is performed during application of the plasticity protocol (gray box). Insets show

(legend continued on next page)

(3.3 ± 1.4 Hz, n = 4) and long-lasting action potentials (>2.5 ms). The CIN firing rate was reduced by ~75% 45 min after intraperitoneal (i.p.) injection of CNO (1 mg/kg), and this decrease in activity remained stable for at least another 30 min (Figure 4B). We then examined the impact of CIN chemogenetic silencing in 6-OHDA hM4Di-injected mice subjected to the rotarod test. Their performance was compared to that of 6-OHDA and non-lesioned mice that received a control AAV carrying only the reporter gene mCherry. All of the experimental groups received CNO (1 mg/kg, i.p.) 45 min before behavioral assessment, so that any potential off-target effects of CNO would affect all of the mice equally (Figure 4C). Since 6-OHDA mice performed poorly in this test, all of the mice were first trained for 5 days to stay on the rotating cylinder when it was spinning at a constant speed (12 rpm, cutoff time 60 s). After the training period, we applied an accelerating protocol for 3 days in which the cylinder speed gradually increased from 4 to 40 rpm in 5 min, which is commonly used to evaluate motor-skill learning in rodents (Giordano et al., 2018; Yin et al., 2009). As previously reported in PD mouse models (Giordano et al., 2018), 6-OHDA mice showed impaired motor-skill learning: while the latency to fall off the rod progressively increased in non-lesioned mice, 6-OHDA mice showed no progress during this period (Figure 4D; Table S2). Chemogenetic inhibition of CINs greatly improved the performance as evidenced by the significant increase in the latency to fall off the cylinder across days in 6-OHDA mice injected with the inhibitory DREADD (Figure 4D; Table S2). These data indicate that reducing CIN activity is an effective way to rescue motor-skill learning in parkinsonian mice.

DISCUSSION

Modulation of corticostriatal transmission by ACh has been inferred primarily from the action of cholinergic receptor agonists in slices experiments. Here, we used an optogenetic approach to probe the effects of endogenous ACh on corticostriatal transmission, focusing on D1 MSNs. A hallmark of CINs is their continuous tonic activity (Bennett and Wilson, 1999; Bennett et al., 2000) and the stereotypical pauses they acquire in response to salient or reward prediction-related stimuli during conditioning (Apicella et al., 1991). Because these features suggest that a brief interruption in CIN firing is a meaningful signal within the striatum, we opted for inhibitory optogenetic tools to manipulate their activity. Our findings provide evidence that acute inhibition of CIN firing potentiates corticostriatal transmission in D1 MSNs in PD-like conditions but not in control conditions. This potentiation is not due to an altered M4 mAChR expression level or activation by endogenous ACh but to the interruption of a PKA-dependent signaling pathway. Furthermore, decreasing CIN firing *in vivo* partially restored LTP at corticostriatal synapses and alleviated motor-skill learning deficits in parkinsonian mice. Overall, these data provide mechanistic insight into the positive effect of anticholinergic strategies in PD.

Previous slice recordings showed that the activation of mAChR reduces excitatory transmission onto MSNs (Ding et al., 2010; Hernandez-Echeagaray et al., 1998; Malenka and Kocsis, 1988; Pancani et al., 2014), and, conversely, one study reported that pharmacological blockade of mAChR modestly increases the amplitude of glutamatergic responses in MSNs (Pakhotin and Bracci, 2007). Because most of these manipulations triggered an alteration in PPR, these effects have been attributed to the activation of pre-synaptic mAChR expressed by cortical terminals (Hersch et al., 1994). Consistently, we also observed a pre-synaptic cholinergic inhibition of corticostriatal transmission when the ACh level was increased by an acetylcholinesterase inhibitor, neostigmine. However, we found that reducing cholinergic tone via the inhibition of CIN firing does not affect cortically evoked EPSPs and PPR in D1 MSNs from non-lesioned mice. This is consistent with the lack of clear effects on behavior and MSN activity reported in several studies upon CIN opto-inhibition (English et al., 2011; Maurice et al., 2015; Ztaou et al., 2018; but see Zucca et al., 2018). The lack of modulation of corticostriatal transmission is not due to insufficient cholinergic tone in slices as opto-inhibition of CINs also failed to modulate EPSPs *in vivo* and our recordings of sIPSCs in GIRK2-overexpressing MSNs showed that phasic activation of post-synaptic mAChR occurred in slices. Therefore, our finding strongly suggests that ACh does not exert a tonic control onto corticostriatal transmission in D1 MSNs at either pre- or post-synaptic levels in non-lesioned mice, which does not exclude phasic activity-dependent modulation in specific behavioral context. In sharp contrast, we found that the brief inhibition of CIN firing significantly increased corticostriatal transmission in D1 MSNs in parkinsonian conditions. These results provide a mechanistic explanation for our previous observation that CIN inhibition in PD mice induces an increased weight of direct pathway in the trans-striatal transfer of cortical information through the basal ganglia (Maurice et al., 2015). In addition, we provided evidence for a post-synaptic site of action. For instance, there was no change in PPR during CIN opto-inhibition, and the preferential antagonist of M4 mAChR, which occluded the potentiation induced by CIN opto-inhibition, substantially increased the amplitude of EPSPs without affecting PPR. These results are fully consistent with a prominent role of post-synaptic M4 mAChR expressed by D1 MSNs. Although we cannot rule out a contribution of brainstem cholinergic afferents, previous results showing that these inputs did not modulate DA release in the striatum, whereas targeted activation of CINs did, strongly suggest that the action of ACh is, at least under certain conditions, primarily mediated by CINs (Brimblecombe et al., 2018; Dautan et al., 2014). We found that EPSP potentiation occurred via a PKA-dependent mechanism. In the striatum, PKA phosphorylation of the GluA1 subunit is increased after pharmacological blockade of M4 mAChR and results in enhanced AMPAR-mediated currents (Mao et al., 2018; Yan et al., 1999).

superimposed averaged EPSPs (n = 8) for individual cells recorded just before (black traces, 1) and 30 min after application of the pairing protocol (color of experimental group, 2).

(D) Summary graph showing the percentage of change in EPSP slope 20–30 min after the pairing protocol (means ± SEMs). Each circle represents an individual cell. **p < 0.01; ns, not significant (averaged last 10 min compared to baseline).

See also Table S2 for statistical information.

Please cite this article in press as: Laverne et al., Cholinergic interneuron inhibition potentiates corticostriatal transmission in direct medium spiny neurons and rescues motor learning in parkinsonism, Cell Reports (2022), https://doi.org/10.1016/j.celrep.2022.111034

CellPress
OPEN ACCESS

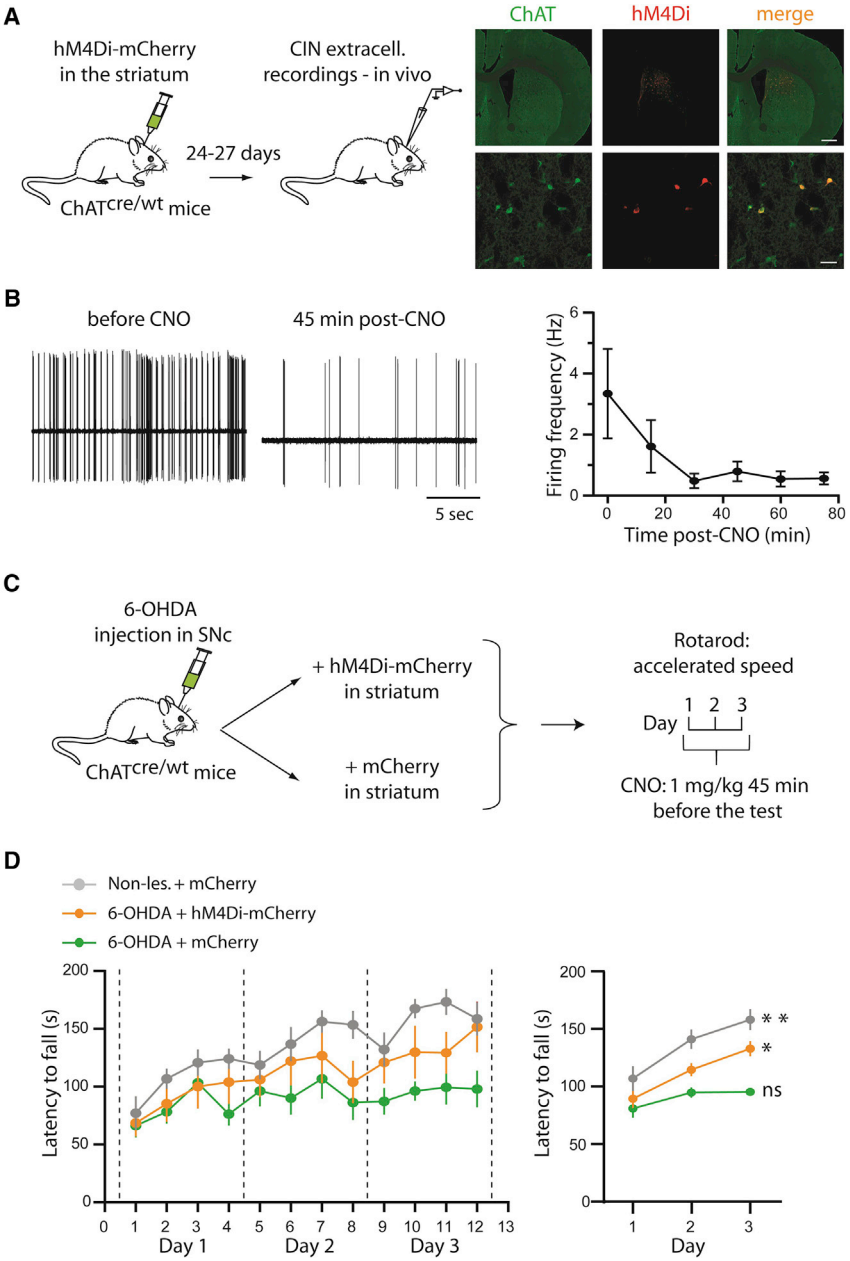

Figure 4. Chemogenetic inhibition of CINs improves motor-skill learning in 6-OHDA mice

(A) Schematic of the *in vivo* recordings in anesthetized mice expressing hM4Di-mCherry and photomicrographs showing the co-localization of DREADD (mCherry, red) with CINs (eGFP, green) in the striatum. Scale bars: top 500 μm, bottom 50 μm.

(B) Representative example of one putative-CIN unit recorded *in vivo* and graph (mean ± SEM) showing the spike frequency of putative CINs before and at several time points after i.p. injection of CNO (1 mg/kg, n = 4).

(C) Schematic of the experimental design for the rotarod test.

(D) Latency to fall off the rotarod (means ± SEMs) across daily trials of each day (left) or averaging trials values (right) in each experimental group (gray: non-lesioned mice injected with AAV-mCherry, n = 9; orange: 6-OHDA mice injected with AAV-hM4Di-mCherry, n = 7; green: 6-OHDA mice injected with AAV-mCherry, n = 14). *p < 0.05; **p < 0.01; ns, not significant. Performances were compared at day 3 versus day 1.

See also Table S2 for statistical information.

It is quite likely that CIN inhibition, by decreasing M4 mAChR stimulation, leads to a similar scenario. A puzzling question is, why is this phenomenon only observed after DA lesion? The most obvious consequence of DA lesion for D1 MSNs is the loss of stimulation of the D1R-mediated signaling pathway, which increases cyclic adenosine monophosphate (cAMP) levels and activates PKA via Gαs/olf proteins, both *in vitro* (Nair et al., 2019) and *in vivo* (Lee et al., 2021). Therefore, because the levels of ACh are elevated relative to DA in the parkinsonian state (McKinley et al., 2019), the system is biased toward activation of Gαi-coupled M4 mAChR, likely resulting in low PKA activity (Lerner and Kreitzer, 2011). In this context, the release of PKA inhibition triggered by CIN silencing would be sufficient to increase AMPAR-mediated responses specifically in parkinsonian mice. Similar disinhibition in healthy conditions would be lessened by the stimulatory effect of D1R and would not be potent enough to modulate MSN glutamatergic responses, at least under basal conditions.

An increase in ACh tone when DA levels fall is a hypothesis often evoked to explain the positive effects of anticholinergic drugs on parkinsonian symptoms. However, the increase in spontaneous CIN activity that would be expected with a hypercholinergic state has not been clearly established in PD models (Tubert and Murer, 2021). Other mechanisms such as aberrant synchronization (Raz et al., 2001), alteration of RGS4-dependent autoreceptors (Ding et al., 2006) or of post-synaptic receptors may explain the increased impact of cholinergic transmission in PD. Here, the use of a direct electrophysiological readout of M4 mAChR activation by endogenous ACh did not reveal major alterations under parkinsonian conditions. Finally, the DA lesion did not affect either the expression of M1 and M4 mAChR in D1 MSNs, reminiscent of the results obtained for nicotinic receptors expressed by thalamic afferences (Tanimura et al., 2019). Overall, given the lack of significant changes in mAChR expression level and sensitivity to endogenous ACh in the parkinsonian state, an imbalance between cholinergic signaling via M4 mAChR and dopaminergic signaling via D1R is probably the most prominent alteration induced by DA lesion in D1 MSNs. This imbalance could result in the tonic inhibition of corticostriatal transmission in these neurons by CINs,

explaining why their optogenetic silencing or the pharmacological blockade of the M4 mAChR potentiates corticostriatal transmission. CIN-mediated tonic inhibition could contribute to the reduction in the strength of corticostriatal synapses observed in D1 MSNs after DA lesion (Fieblinger et al., 2014). Interestingly, a previous work demonstrated that the loss of D2R signaling contributed to the amplification by CINs of thalamic-evoked responses in D2 MSNs in parkinsonian mice (Tanimura et al., 2019). Together, these data suggest that the suppression of DA action on D1R and D2R increases the strength of the control exerted by CINs on corticostriatal and thalamostriatal transmission in parkinsonian state.

Long-term changes in the synaptic strength of corticostriatal synapses are believed to represent the cellular substrate of sensorimotor learning (Di Filippo et al., 2009; Graybiel, 1998; Pisani et al., 2005). More precisely, the dorsolateral striatum that receives projections from somatosensory and motor cortical areas has been implicated in the acquisition and performance of motor sequences and could be activated during all stages of incremental motor learning (Giordano et al., 2018; Thorn et al., 2010; but see Yin et al., 2009). We therefore recorded MSNs in the dorsolateral area of the striatum and found that a Hebbian protocol induced corticostriatal LTP in a majority of MSNs in non-lesioned mice, in agreement with earlier works (Charpier and Deniau, 1997; Fisher et al., 2017). In contrast, MSNs from parkinsonian mice no longer exhibited LTP. The loss of LTP in slices from parkinsonian mice has long been reported (Centonze et al., 1999; Picconi et al., 2003), and here, we report that this form of plasticity is also lost *in vivo* after chronic DA lesion. We and others have previously shown that the targeted inhibition of CINs improved the performance of parkinsonian mice in motor tasks that do not have a strong learning component (Maurice et al., 2015; Tanimura et al., 2019; Ztaou et al., 2016). Our present result demonstrating that chemogenetically induced decrease in CIN firing enabled parkinsonian mice to significantly improve their performance over time in the accelerating rotarod task extends this notion to motor-skill learning. Considering that corticostriatal LTP is induced by motor learning in the dorsolateral striatum (Giordano et al., 2018), our working hypothesis is that CIN inhibition improves motor learning in parkinsonian mice through their ability to induce LTP at corticostriatal synapses, as observed here in some MSNs. We showed that decreasing cholinergic tone in M4 mAChR potentiates basal corticostriatal transmission via a PKA-dependent mechanism in D1 MSNs. Interestingly, PKA is also activated in these neurons in the early learning stages (Lee et al., 2021), and this activation could promote PKA-dependent LTP (Picconi et al., 2003). LTP induction is instead abolished in D1 MSNs when M4 mAChR signaling is boosted with a positive allosteric modulator (Shen et al., 2015). These results suggest that the inhibition of CIN firing in the parkinsonian state may favor PKA-dependent LTP in D1 MSNs by lowering M4 mAChR activation.

While further studies are needed to fully understand how CINs affect the striatal network in normal and pathological conditions, our data reveal the existence of abnormal cholinergic responsiveness in D1 MSNs in the parkinsonian state that affects corticostriatal transmission. They also suggest that targeting CIN firing is a valuable therapeutic option that avoids extrastriatal and unspecific effects of anticholinergic drugs (Paz and Murer, 2021).

Limitations of the study

Because of the low throughput and difficulty in obtaining high-quality long-lasting intracellular recordings *in vivo*, especially in 6-OHDA mice, we were unable to identify the type of MSNs exhibiting LTP under CIN opto-inhibition, which prevented us from establishing a causal relationship between the *in vitro* and *in vivo* electrophysiological results. Furthermore, although we did not show major changes in the activation of M4 mAChR by endogenous ACh in parkinsonian mice, it would be interesting in the future to quantify ACh levels with genetically encoded sensors to determine the impact of the DA lesion on ACh release, as this issue remains quite controversial.

STAR★METHODS

Detailed methods are provided in the online version of this paper and include the following:

- KEY RESOURCES TABLE
- RESOURCE AVAILABILITY
  - Lead contact
  - Materials availability
  - Data and code availability
- EXPERIMENTAL MODEL AND SUBJECT DETAILS
  - Experimental models
  - Stereotaxic surgery
- METHOD DETAILS
  - Slice preparation
  - *In vitro* electrophysiology
  - *In vivo* electrophysiology
  - Immunohistochemistry
  - FACS-sorting
  - RNA extraction
  - Reverse transcription followed by quantitative polymerase chain reaction (RT-qPCR)
  - Western blotting and quantification
  - Rotarod
- QUANTIFICATION AND STATISTICAL ANALYSIS

SUPPLEMENTAL INFORMATION

Supplemental information can be found online at https://doi.org/10.1016/j.celrep.2022.111034.

ACKNOWLEDGMENTS

This work was funded by grants from Fondation de France and Association France Parkinson. It was supported by the Center National de la Recherche Scientifique (CNRS), Aix-Marseille University (AMU), and the French government under the program Investissements d'Avenir, Initiative d'Excellence d'Aix-Marseille Université via A*Midex funding (NeuroMarseille, AMX-19-IET-004), and ANR (ANR-17-EURE-0029). J.P. was supported by a PhD fellowship from the Ministry of Higher Education, Research, and Innovation. We thank Pascal Salin for his precious help with immunohistochemistry; Catherine Lepolard for performing western blot experiments; Jean-Pierre Kessler for

statistical analysis; and Maxime Assous, Aziz Moqrich, and Hélène Marie for their critical comments on the manuscript. We also want to thank Raphael Vallat, Fabien Tell, and Hamza Oueld Kaddour El Hallaoui for their precious help with mixed models.

AUTHOR CONTRIBUTIONS

A.R., L.K.-L.G., N.M., and C.B. designed the study. G.L., J.P., A.R., C.M., E.G., N.M., and C.B. performed the experiments. G.L., J.P., A.R., E.C., N.M., and C.B. analyzed the results. N.M. and C.B. contributed to funding acquisition. C.B. wrote the manuscript, with the participation of N.M. and L.K.-L.G. All of the authors read and approved the submission.

DECLARATION OF INTERESTS

The authors declare no competing financial interests.

Received: July 29, 2021
Revised: April 27, 2022
Accepted: June 11, 2022
Published: July 5, 2022

REFERENCES

Abudukeyoumu, N., Hernandez-Flores, T., Garcia-Munoz, M., and Arbuthnott, G.W. (2019). Cholinergic modulation of striatal microcircuits. Eur. J. Neurosci. *49*, 604–622. https://doi.org/10.1111/ejn.13949.

Albin, R.L., Young, A.B., and Penney, J.B. (1989). The functional anatomy of basal ganglia disorders. Trends Neurosci. *12*, 366–375. https://doi.org/10.1016/0166-2236(89)90074-x.

Aosaki, T., Tsubokawa, H., Ishida, A., Watanabe, K., Graybiel, A.M., Kimura, M., and IshidA, A. (1994a). Responses of tonically active neurons in the primate's striatum undergo systematic changes during behavioral sensorimotor conditioning. J. Neurosci. *14*, 3969–3984. https://doi.org/10.1523/jneurosci.14-06-03969.1994.

Aosaki, T., Graybiel, A.M., and Kimura, M. (1994b). Effect of the nigrostriatal dopamine system on acquired neural responses in the striatum of behaving monkeys. Science *265*, 412–415. https://doi.org/10.1126/science.8023166.

Aosaki, T., Kimura, M., and Graybiel, A.M. (1995). Temporal and spatial characteristics of tonically active neurons of the primate's striatum. J. Neurophysiol. *73*, 1234–1252. https://doi.org/10.1152/jn.1995.73.3.1234.

Apicella, P., Scarnati, E., and Schultz, W. (1991). Tonically discharging neurons of monkey striatum respond to preparatory and rewarding stimuli. Exp. Brain Res. *84*, 672–675. https://doi.org/10.1007/bf00230981.

Apicella, P., Scarnati, E., Ljungberg, T., and Schultz, W. (1992). Neuronal activity in monkey striatum related to the expectation of predictable environmental events. J. Neurophysiol. *68*, 945–960. https://doi.org/10.1152/jn.1992.68.3.945.

Bennett, B.D., and Wilson, C.J. (1999). Spontaneous activity of neostriatal cholinergic interneurons *in vitro*. J. Neurosci. *19*, 5586–5596. https://doi.org/10.1523/jneurosci.19-13-05586.1999.

Bennett, B.D., Callaway, J.C., and Wilson, C.J. (2000). Intrinsic membrane properties underlying spontaneous tonic firing in neostriatal cholinergic interneurons. J. Neurosci. *20*, 8493–8503. https://doi.org/10.1523/jneurosci.20-22-08493.2000.

Brimblecombe, K.R., Threlfell, S., Dautan, D., Kosillo, P., Mena-Segovia, J., and Cragg, S.J. (2018). Targeted activation of cholinergic interneurons accounts for the modulation of dopamine by striatal nicotinic receptors. Eneuro *5*. https://doi.org/10.1523/eneuro.0397-17.2018.

Centonze, D., Gubellini, P., Picconi, B., Calabresi, P., Giacomini, P., and Bernardi, G. (1999). Unilateral dopamine denervation blocks corticostriatal LTP. J. Neurophysiol. *82*, 3575–3579. https://doi.org/10.1152/jn.1999.82.6.3575.

Charpier, S., and Deniau, J.M. (1997). In vivo activity-dependent plasticity at cortico-striatal connections: evidence for physiological long-term potentiation. Proc. Natl. Acad. Sci. USA *94*, 7036–7040. https://doi.org/10.1073/pnas.94.13.7036.

Dautan, D., Huerta-Ocampo, I., Witten, I.B., Deisseroth, K., Bolam, J.P., Gerdjikov, T., and Mena-Segovia, J. (2014). A major external source of cholinergic innervation of the striatum and nucleus accumbens originates in the brainstem. J. Neurosci. *34*, 4509–4518. https://doi.org/10.1523/jneurosci.5071-13.2014.

DeLong, M.R. (1990). Primate models of movement disorders of basal ganglia origin. Trends Neurosci. *13*, 281–285. https://doi.org/10.1016/0166-2236(90)90110-v.

Ding, J., Guzman, J.N., Tkatch, T., Chen, S., Goldberg, J.A., Ebert, P.J., Levitt, P., Wilson, C.J., Hamm, H.E., and Surmeier, D.J. (2006). RGS4-dependent attenuation of M4 autoreceptor function in striatal cholinergic interneurons following dopamine depletion. Nat. Neurosci. *9*, 832–842. https://doi.org/10.1038/nn1700.

Ding, J.B., Guzman, J.N., Peterson, J.D., Goldberg, J.a., and Surmeier, D.J. (2010). Thalamic gating of corticostriatal signaling by cholinergic interneurons. Neuron *67*, 294–307. https://doi.org/10.1016/j.neuron.2010.06.017.

English, D.F., Ibanez-Sandoval, O., Stark, E., Tecuapetla, F., Buzsáki, G., Deisseroth, K., Tepper, J.M., and Koos, T. (2011). GABAergic circuits mediate the reinforcement-related signals of striatal cholinergic interneurons. Nat. Neurosci. *15*, 123–130. https://doi.org/10.1038/nn.2984.

Fieblinger, T., Graves, S.M., Sebel, L.E., Alcacer, C., Plotkin, J.L., Gertler, T.S., Chan, C.S., Heiman, M., Greengard, P., Cenci, M.A., and Surmeier, D.J. (2014). Cell type-specific plasticity of striatal projection neurons in parkinsonism and L-DOPA-induced dyskinesia. Nat. Commun. *5*, 5316. https://doi.org/10.1038/ncomms6316.

Di Filippo, M., Picconi, B., Tantucci, M., Ghiglieri, V., Bagetta, V., Sgobio, C., Tozzi, A., Parnetti, L., and Calabresi, P. (2009). Short-term and long-term plasticity at corticostriatal synapses: implications for learning and memory. Behav. Brain Res. *199*, 108–118. https://doi.org/10.1016/j.bbr.2008.09.025.

Fisher, S.D., Robertson, P.B., Black, M.J., Redgrave, P., Sagar, M.A., Abraham, W.C., and Reynolds, J.N.J. (2017). Reinforcement determines the timing dependence of corticostriatal synaptic plasticity *in vivo*. Nat. Commun. *8*, 334. https://doi.org/10.1038/s41467-017-00394-x.

Giordano, N., Iemolo, A., Mancini, M., Cacace, F., De Risi, M., Latagliata, E.C., Ghiglieri, V., Bellenchi, G.C., Puglisi-Allegra, S., Calabresi, P., et al. (2018). Motor learning and metaplasticity in striatal neurons: relevance for Parkinson's disease. Brain *141*, 505–520. https://doi.org/10.1093/brain/awx351.

Goldberg, J.A., and Reynolds, J.N.J. (2011). Spontaneous firing and evoked pauses in the tonically active cholinergic interneurons of the striatum. Neuroscience *198*, 27–43. https://doi.org/10.1016/j.neuroscience.2011.08.067.

Randall, P.A., McElligott, Z.A., and Besheer, J. (2012). Muscarinic modulation of striatal function and circuitry. Handb. Exp. Pharmacol., *223*. https://doi.org/10.1111/adb.12782.

Graybiel, A.M. (1998). The basal ganglia and chunking of action repertoires. In Neurobiology of Learning and Memory (Academic Press Inc.), pp. 119–136.

Hernández-Echeagaray, E., Galarraga, E., and Bargas, J. (1998). 3-Alpha-chloro-imperialine, a potent blocker of cholinergic presynaptic modulation of glutamatergic afferents in the rat neostriatum. Neuropharmacology *37*, 1493–1502. https://doi.org/10.1016/s0028-3908(98)00131-2.

Hernández-Flores, T., Hernández-González, O., Pérez-Ramírez, M.B., Lara-González, E., Arias-García, M.A., Duhne, M., Pérez-Burgos, A., Prieto, G.A., Figueroa, A., Galarraga, E., and Bargas, J. (2015). Modulation of direct pathway striatal projection neurons by muscarinic M_4-type receptors. Neuropharmacology *89*, 232–244. https://doi.org/10.1016/j.neuropharm.2014.09.028.

Hersch, S.M., Gutekunst, C.A., Rees, H.D., Heilman, C.J., and Levey, A.I. (1994). Distribution of m1-m4 muscarinic receptor proteins in the rat striatum: light and electron microscopic immunocytochemistry using subtype-specific antibodies. J. Neurosci. *14*, 3351–3363. https://doi.org/10.1523/jneurosci.14-05-03351.1994.

Lee, S.J., Lodder, B., Chen, Y., Patriarchi, T., Tian, L., and Sabatini, B.L. (2021). Cell-type-specific asynchronous modulation of PKA by dopamine in learning. Nature *590*, 451–456. https://doi.org/10.1038/s41586-020-03050-5.

Lenth, R., Singmann, H., Love, J., Buerkner, P., and Herve, M. (2018). Emmeans: estimated marginal means, aka least-squares means. R Packag. Vers *1*, 3.

Lerner, T.N., and Kreitzer, A.C. (2011). Neuromodulatory control of striatal plasticity and behavior. Curr. Opin. Neurobiol. *21*, 322–327. https://doi.org/10.1016/j.conb.2011.01.005.

Mahon, S. (2001). Relationship between EEG potentials and intracellular activity of striatal and cortico-striatal neurons: an *in vivo* study under different anesthetics. Cerebr. Cortex *11*, 360–373.

Malenka, R.C., and Kocsis, J.D. (1988). Presynaptic actions of carbachol and adenosine on corticostriatal synaptic transmission studied *in vitro*. J. Neurosci. *8*, 3750–3756. https://doi.org/10.1523/jneurosci.08-10-03750.1988.

Mallet, N., Le Moine, C., Charpier, S., and Gonon, F. (2005). Feedforward inhibition of projection neurons by fast-spiking GABA interneurons in the rat striatum *in vivo*. J. Neurosci. *25*, 3857–3869.

Mamaligas, A.A., and Ford, C.P. (2016). Spontaneous synaptic activation of muscarinic receptors by striatal cholinergic neuron firing. Neuron *91*, 574–586. https://doi.org/10.1016/j.neuron.2016.06.021.

Mao, L.M., He, N., Jin, D.Z., and Wang, J.Q. (2018). Regulation of phosphorylation of AMPA glutamate receptors by muscarinic M4 receptors in the striatum *in vivo*. Neuroscience *375*, 84–93. https://doi.org/10.1016/j.neuroscience.2018.01.063.

Maurice, N., Liberge, M., Jaouen, F., Ztaou, S., Hanini, M., Camon, J., Deisseroth, K., Amalric, M., Kerkerian-Le Goff, L., and Beurrier, C. (2015). Striatal cholinergic interneurons control motor behavior and basal ganglia function in experimental parkinsonism. Cell Rep. *13*, 657–666. https://doi.org/10.1016/j.celrep.2015.09.034.

McKinley, J.W., Shi, Z., Kawikova, I., Hur, M., Bamford, I.J., Sudarsana Devi, S.P., Vahedipour, A., Darvas, M., and Bamford, N.S. (2019). Dopamine deficiency reduces striatal cholinergic interneuron function in models of Parkinson's disease. Neuron *103*, 1056–1072.e6. https://doi.org/10.1016/j.neuron.2019.06.013.

Nair, A.G., Castro, L.R.V., El Khoury, M., Gorgievski, V., Giros, B., Tzavara, E.T., Hellgren-Kotaleski, J., and Vincent, P. (2019). The high efficacy of muscarinic M4 receptor in D1 medium spiny neurons reverses striatal hyperdopaminergia. Neuropharmacology *146*, 74–83. https://doi.org/10.1016/j.neuropharm.2018.11.029.

Pakhotin, P., and Bracci, E. (2007). Cholinergic interneurons control the excitatory input to the striatum. J. Neurosci. *27*, 391–400. https://doi.org/10.1523/jneurosci.3709-06.2007.

Pancani, T., Bolarinwa, C., Smith, Y., Lindsley, C.W., Conn, P.J., and Xiang, Z. (2014). M4 mAChR-mediated modulation of glutamatergic transmission at corticostriatal synapses. ACS Chem. Neurosci. *5*, 318–324. https://doi.org/10.1021/cn500003z.

Paz, R.M., and Murer, M.G. (2021). Mechanisms of antiparkinsonian anticholinergic therapy revisited. Neuroscience *467*, 201–217. https://doi.org/10.1016/j.neuroscience.2021.05.026.

Picconi, B., Centonze, D., Håkansson, K., Bernardi, G., Greengard, P., Fisone, G., Cenci, M.A., and Calabresi, P. (2003). Loss of bidirectional striatal synaptic plasticity in L-DOPA-induced dyskinesia. Nat. Neurosci. *6*, 501–506. https://doi.org/10.1038/nn1040.

Pisani, A., Centonze, D., Bernardi, G., and Calabresi, P. (2005). Striatal synaptic plasticity: implications for motor learning and Parkinson's disease. Mov. Disord. *20*, 395–402. https://doi.org/10.1002/mds.20394.

R Core Team (2013). R: A Language and Environment for Statistical Computing. (R Foundation for Statistical Computing, Vienna). http://www.R-project.org/.

Raz, A., Frechter-Mazar, V., Feingold, A., Abeles, M., Vaadia, E., and Bergman, H. (2001). Activity of pallidal and striatal tonically active neurons is correlated in mptp-treated monkeys but not in normal monkeys. J. Neurosci. *21*, RC128. https://doi.org/10.1523/jneurosci.21-03-j0006.2001.

Schulz, J.M., Redgrave, P., and Reynolds, J.N.J. (2010). Cortico-striatal spike-timing dependent plasticity after activation of subcortical pathways. Front. Synaptic Neurosci. *2*, 150. https://doi.org/10.3389/fnsyn.2010.00150.

Shen, W., Plotkin, J.L., Francardo, V., Ko, W.K.D., Xie, Z., Li, Q., Fieblinger, T., Wess, J., Neubig, R.R., Lindsley, C.W., et al. (2015). M4 muscarinic receptor signaling ameliorates striatal plasticity deficits in models of L-DOPA-induced dyskinesia. Neuron *88*, 762–773. https://doi.org/10.1016/j.neuron.2015.10.039.

Smith, Y., Bevan, M.D., Shink, E., and Bolam, J.P. (1998). Microcircuitry of the direct and indirect pathways of the basal ganglia. Neuroscience *86*, 353–387. https://doi.org/10.1016/s0306-4522(98)00004-9.

Tanimura, A., Du, Y., Kondapalli, J., Wokosin, D.L., and Surmeier, D.J. (2019). Cholinergic interneurons amplify thalamostriatal excitation of striatal indirect pathway neurons in Parkinson's disease models. Neuron *101*, 444–458.e6. https://doi.org/10.1016/j.neuron.2018.12.004.

Thorn, C.A., Atallah, H., Howe, M., and Graybiel, A.M. (2010). Differential dynamics of activity changes in dorsolateral and dorsomedial striatal loops during learning. Neuron *66*, 781–795.

Tubert, C., and Murer, M.G. (2021). What's wrong with the striatal cholinergic interneurons in Parkinson's disease? Focus on intrinsic excitability. Eur. J. Neurosci. *53*, 2100–2116.

Yan, Z., Hsieh-Wilson, L., Feng, J., Tomizawa, K., Allen, P.B., Fienberg, A.A., Nairn, A.C., and Greengard, P. (1999). Protein phosphatase 1 modulation of neostriatal AMPA channels: regulation by DARPP-32 and spinophilin. Nat. Neurosci. *2*, 13–17. https://doi.org/10.1038/4516.

Yan, Z., Flores-Hernandez, J., and Surmeier, D.J. (2001). Coordinated expression of muscarinic receptor messenger RNAs in striatal medium spiny neurons. Neuroscience *103*, 1017–1024. https://doi.org/10.1016/s0306-4522(01)00039-2.

Yin, H.H., Mulcare, S.P., Hilário, M.R.F., Clouse, E., Holloway, T., Davis, M.I., Hansson, A.C., Lovinger, D.M., and Costa, R.M. (2009). Dynamic reorganization of striatal circuits during the acquisition and consolidation of a skill. Nat. Neurosci. *12*, 333–341. https://doi.org/10.1038/nn.2261.

Zhai, S., Tanimura, A., Graves, S.M., Shen, W., and Surmeier, D.J. (2018). Striatal synapses, circuits, and Parkinson's disease. Curr. Opin. Neurobiol. *48*, 9–16. https://doi.org/10.1016/j.conb.2017.08.004.

Ztaou, S., Maurice, N., Camon, J., Guiraudie-Capraz, G., Kerkerian-Le Goff, L., Beurrier, C., Liberge, M., and Amalric, M. (2016). Involvement of striatal cholinergic interneurons and M1 and M4 muscarinic receptors in motor symptoms of Parkinson's disease. J. Neurosci. *36*, 9161–9172. https://doi.org/10.1523/jneurosci.0873-16.2016.

Ztaou, S., Lhost, J., Watabe, I., Torromino, G., and Amalric, M. (2018). Striatal cholinergic interneurons regulate cognitive and affective dysfunction in partially dopamine-depleted mice. Eur. J. Neurosci. *48*, 2988–3004. https://doi.org/10.1111/ejn.14153.

Zucca, S., Zucca, A., Nakano, T., Aoki, S., and Wickens, J. (2018). Pauses in cholinergic interneuron firing exert an inhibitory control on striatal output *in vivo*. Elife *7*, e32510. https://doi.org/10.7554/elife.32510.

Please cite this article in press as: Laverne et al., Cholinergic interneuron inhibition potentiates corticostriatal transmission in direct medium spiny neurons and rescues motor learning in parkinsonism, Cell Reports (2022), https://doi.org/10.1016/j.celrep.2022.111034

CellPress
OPEN ACCESS

STAR★METHODS

KEY RESOURCES TABLE

REAGENT or RESOURCE	SOURCE	IDENTIFIER
Antibodies		
Rabbit anti-GFP	Thermo Fischer Scientific	Cat# A-11122; RRID: AB_221569
Goat anti-ChAT	Millipore	Cat# AB144P; RRID: AB_2079751
Mouse anti-TH, clone LNC1	Millipore	Cat# MAB318; RRID: AB_2201528
Rabbit anti-RFP	MBL International	Cat# PM005; RRID: AB_591279
Rabbit anti-GIRK2	Alomone labs	Cat# APC-006; RRID: AB_2040115
Rabbit anti-GADPH	Abcam	Cat# Ab9485; RRID: AB_307275
Donkey anti-rabbit Alexa Fluor 488	Thermo Fischer Scientific	Cat# A21206; RRID: AB_2535792
Donkey anti-goat Alexa Fluor 594	Thermo Fischer Scientific	Cat# A32758; RRID: AB_2762828
Goat anti-mouse Horseradish peroxidase (HRP)-conjugated	Jackson ImmunoResearch	Cat# 115-065-166; RRID: AB_2338569
Donkey anti-rabbit Alexa Fluor 555	Thermo Fischer Scientific	Cat# A31572; RRID: AB_162543
Goat anti-mouse Horseradish peroxidase (HRP)-conjugated	Abcam	Cat# Ab205719; RRID: AB_2755049
Goat anti-rabbit Horseradish peroxidase (HRP)-conjugated	Cell Signaling Technology	Cat# 7074; RRID: AB_2099233
Bacterial and virus strains		
AAV9.hSyn.tdTomato.T2A.mGIRK2-1	Penn Vector Core	V7335S
AAV8-hSyn-DIO-hM4D(Gi)-mCherry	Addgene	Cat# 44362-AAV8; RRID: Addgene_44362
AAV8-hSyn-DIO-mCherry	Addgene	Cat# 50459-AAV8; RRID: Addgene_50459
Chemicals, peptides, and recombinant proteins		
6-Hydroxydopamine hydrochloride	Sigma-Aldrich	Cat# H4381; CAS# 28094-15-7
Picrotoxin	Tocris	Cat# 1128; CAS# 124-87-8
PKA inhibitor fragment (6-22) amide	Tocris	Cat# 1904; CAS# 121932-06-7
Tropicamide	Tocris	Cat# 0909; CAS# 1508-75-4
Clozapine N-oxide dihydrochloride	Tocris	Cat# 6329; CAS# 2250025-93-3
Carbachol	Sigma-Aldrich	Cat# C4382; CAS# 51-83-2
Neostigmine bromide	Sigma-Aldrich	Cat# N2001; CAS# 114-80-7
Critical commercial assays		
Syber Green ROX master mix	Thermofisher	Cat# K0221
RNeasy Micro Kit	Quiagen	Cat# 73934
Vectastain Elite ABC-HRP Kit, Peroxidase Standard	Vector Laboratories	Cat# PK-6100
Immobilon Western Chemiluminescent HRP Substrate	Millipore	Cat# WBKLS
Experimental models: Organisms/strains		
Mouse/ChAT-Cre	Jackson Laboratory	Strain# 006410; RRID:IMSR_JAX:006410
Mouse/Rosa26-NpHR	Jackson Laboratory	Strain# 014539; RRID:IMSR_JAX:014539
Mouse/D1-tdTomato	Jackson Laboratory	Strain# 016204; RRID:IMSR_JAX:016204
Oligonucleotides		
Chrma1-Fw: AAGATGGATTGAATGAGGCTGC	This paper	N/A
Chrma1-Rse: CCTCCAGTCACAAGATTTTTCTCA	This paper	N/A
Chrma4-Fw: CAGCGGAGCAAGACAGAAG	This paper	N/A

(*Continued on next page*)

Continued

REAGENT or RESOURCE	SOURCE	IDENTIFIER
Chrma4-Rse: CATTGACAGGTGTGAAGTTCG	This paper	N/A
Gapdh-Fw: ATGGTGAAGGTCGGTGTGA	This paper	N/A
Gapdh-Rse: AATCTCCACTTTGCCACTGC	This paper	N/A
Software and algorithms		
GraphPad Prism 9	GraphPad Software	RRID:SCR_002798 http://www.graphpad.com/
Spike2 Software	Cambridge Electronic Device	RRID:SCR_000903 https://ced.co.uk/
pClamp 10.7	Molecular Devices	RRID:SCR_011323 https://www.moleculardevices.com
Adobe Illustrator CS	Adobe	RRID:SCR_010279 https://www.adobe.com/products/illustrator.html
R Project for Statistical Computing	R project	RRID:SCR_001905 https://www.r-project.org/
R package: nlme	R software package	RRID:SCR_015655 https://cran.r-project.org/web/packages/nlme/index.html
R package: emmeans	R software package	RRID:SCR_018734 https://cran.r-project.org/web/packages/emmeans/index.html

RESOURCE AVAILABILITY

Lead contact

Further information and requests for resources and reagent should be direct to and will be fulfilled by the Lead Contact, Corinne Beurrier (Corinne.beurrier@univ-amu.fr)

Materials availability

This study did not generate new unique reagents.

Data and code availability

All data reported in this paper will be shared by the lead contact upon request.

This paper does not report original code.

Any additional information required to reanalyze the data reported in this paper is available from the lead contact upon request.

EXPERIMENTAL MODEL AND SUBJECT DETAILS

Experimental models

All mice strains used in this study were purchased from Jackson Laboratory). Mice were 2–4 months old at the time of experiments. We used Choline acetyltransferase ChAT-IRES-Cre knock-in mice (stock number: 006410) and LoxP-stop-eNpHR3.0-EYFP mice (stock number: 014539). Homozygotes from each strain were crossed in-house to produce heterozygous, double-transgenic $ChAT^{cre/wt}$;$Rosa^{NpHR/wt}$ offspring and were used for *in vivo* electrophysiology. For *in vitro* electrophysiological experiments requiring D1 MSN identification and NpHR expression in cholinergic neurons, homozygous $ChAT^{cre/cre}$ mice were first crossed with BAC Drd1a-tdTomato mice (D1-tdTomato mice, stock number: 016204). Double transgenic offspring ($ChAT^{cre/wt}$;D1-tdTomato$^{+/-}$) were then crossed with homozygotes $Rosa^{NpHR/NpHR}$ to produce about one quarter of triple-transgenic $ChAT^{cre/wt}$;D1-tdTomato$^{+/-}$;$Rosa^{NpHR/wt}$ mice. To provide chemogenetic inhibition of CINs, AAV containing the inhibitory DREADDs was injected into the striatum of heterozygous $ChAT^{cre/wt}$ mice. Both adult male and female mice were used in this study. Animals were housed 3–5 per cage (1–2 per cage if animals underwent surgical procedures), maintained under standard housing conditions (12-h light/dark cycles, 23°C, 40% humidity) with unrestricted access to food and water and monitored daily by animal care technicians and research staff. All procedures agreed with European Union recommendations for animal experimentation (2010/63/EU) and were approved by the national and local ethical committees (Marseille ethics committee # 14). The project authorization is registered under the number 2019022216247615-V3 #19414 delivered by the French Ministry of Higher Education, Research and Innovation.

Stereotaxic surgery

Mice were anesthetized with intraperitoneal (i.p.) injections of ketamine and xylazine (100 and 10 mg/kg, respectively) and mounted on a stereotaxic apparatus (Kopf Instruments). Injections were made with a 10-μL syringe, connected to a 33- or 34-gauge needle injector by a polyethylene tubing, and controlled by an injection pump at 0.3 μL/min. All stereotaxic coordinates are calculated relative to bregma. Mice received one unilateral injection of 6-OHDA hydrochloride (1.5 μL at 2.7 μg/μL diluted in 0.9% sterile NaCl containing 0.1% ascorbic acid, Sigma-Aldrich) into the substantia nigra pars compacta (−3.0 mm AP, ±1.3 mm ML, −4.3 mm DV). For cre-dependent hM4Di-mcherry expression in CINs, 6-OHDA injection was immediately followed by unilateral injection of AAV8-hSyn-DIO-hM4D(Gi)-mCherry (2.9 × 10^{13} GC/mL, Addgene) into the striatum ipsilateral to the lesioned side of $ChAT^{cre/wt}$ mice. Injections were performed at four sites (0.75 μL per site) at the following coordinates: +1.1 mm AP, ±1.7 mm ML, −2.7 and −2.1 mm DV and +0.38 mm AP, ±1.9 mm ML, −2.7 and −2.1 mm DV. The control virus (AAV8-hSyn-DIO-mCherry, 2.3 × 10^{13} GC/mL, Addgene) was injected according to the same procedure. To express GIRK2 in MSNs, unilateral injection of AAV9-hSyn-tdTomato-GIRK2 (0.5 μL) were performed into the striatum ipsilateral to the 6-OHDA-lesioned side (+0.8 mm AP, ±1.8 mm ML, −2.5 mm DV) (AAV9.hSyn.tdTomato.T2A.mGIRK2-1-A22A.WPRE.bGH, 4.42 × 10^{13} GC/mL, Penn Vector Core). After injections, the needle was left in place for 10 min before removal. The scalp was then sutured and animals were maintained on a heating pad until they fully recovered from anesthesia. Rimadyl (5 mg/kg) was administered subcutaneously for post-operative analgesia over 24–48 h, including the day of surgery.

METHOD DETAILS

Slice preparation

Mice were deeply anesthetized with ketamine/xylazine (100/10 mg/kg, i.p.) and transcardially perfused with an ice-cold N-methyl D-glucamine (NMDG)-based solution containing (in mM): 93 NMDG, 2.5 KCl, 1.2 NaH_2PO_4, 30 $NaHCO_3$, 20 HEPES, 20 glucose, 10 $MgCl_2$, 93 HCl, 2 Thiourea, 3 sodium pyruvate, 12 N-acetyl cysteine and 0.5 $CaCl_2$ (saturated with 95% O_2 and 5% CO_2, pH 7.2–7.4). The brain was then removed from the skull and glued to the stage of a vibratome (Leica, VT1000S) where it remained submerged in ice-cold oxygenated NMDG-based solution. Coronal slices (250 μm thick) containing the striatum were collected. Slices were immediately transferred to recover in NMDG-based solution at 35°C for 5 min and then stored for at least 1 h at room temperature in normal artificial cerebrospinal fluid (ACSF) containing (in mM): 126 NaCl, 2.5 KCl, 1.2 MgCl2, 1.2 NaH2PO4, 2.4 CaCl2, 25 NaHCO3 and 11 glucose, to which 250 μM kynurenic acid and 1 mM sodium pyruvate had been added. For the recordings, slices were transferred one at a time to a submersion-type chamber and perfused continuously with warm ACSF (32–34°C) at a rate of 3 mL/min. Solutions were continuously equilibrated with 95% O2/5% CO2. In all experiments picrotoxin (50 μM) was included in the ACSF to block $GABA_A$ receptors. For PKA inhibition in D1 MSNs, the membrane impermeable nonmyristoylated form of PKA inhibitor (PKI 6-22 amide, 20 μM) was added to the intra-pipette solution. All compounds were purchased from Tocris or Sigma-Aldrich.

In vitro electrophysiology

Neurons were visualized on an upright microscope (Nikon Eclipse FN1) equipped with DIC optic and filters set to visualize tdTomato and EYFP using an IR 40× water-immersion objective (Nikon). Combination of electrophysiological properties and expression of fluorophore was used to identify CINs and D1 MSNs. Patch-clamp recordings were performed in whole-cell configurations in current-clamp mode. Patch-clamp electrodes (4–6 MΩ) were prepared from filamented borosilicate glass capillaries (PG150T-7.5, Harvard Apparatus) using a micropipette puller (PC-10, Narishige) and were filled with an intracellular solution containing (in mM): 126 KMeSO4, 14 KCl, 3 MgCl2, 0.5 CaCl2, 5 EGTA, 10 HEPES, 2 NaATP and 0.5 mM NaGTP, 10 Na-Phosphocreatine, pH adjusted to 7.25 with NaOH and osmolarity adjusted to 270–280 mOsm/L.

Recordings were obtained using motorized micromanipulators (MP-85, Sutter Instrument), a Multiclamp 700B amplifier, a Digidata 1550B digitizer, and pClamp 10.7 acquisition software (Molecular Devices, San Jose, CA, USA). Signals were low-pass filtered at 10 kHz online and sampled at 10 kHz. Electrode capacitances were compensated electronically during recording. In current-clamp mode, the bridge was continuously balanced and input resistances were monitored with a 50-pA negative step given with every afferent stimulus. Cells showing more than 20% of input resistance variation were excluded from the analysis. To evoke EPSPs in MSNs, electrical stimulation of cortical afferents was performed using a bipolar tungsten electrode placed in the corpus callosum at the border of the cortex and the striatum. As the characteristics of CINs and MSNs can vary according to the territories of the striatum, recordings were restricted to the dorsolateral region of the striatum. The intensity of the electrical stimulations performed by current pulses (0.1-ms width every 10 s) was adjusted to obtain EPSPs with an amplitude approximately equal to 50% of the maximum response. Optogenetic stimulation of eNpHR-expressing CINs was delivered under the control of the acquisition software via the microscope objective lens using wide-field 585 nm LED illumination (Spectra Light Engine, Lumencor, Optoprim). In the majority of experiments examining the effects of CIN photoinhibition on EPSPs, light stimulation was delivered as a 150-ms width pulse. Paired-cortical stimulation (50 ms interstimulus interval) started 50 ms after light was turned on. EPSP amplitudes were calculated by taking the maximum peak amplitude and comparing this with the mean of a 10-ms window immediately before the stimulation artifact. For 6-OHDA injected mice, recordings were performed 20 to 36 days post-injection. For AAV-GIRK2 injected-mice, recordings were performed 26 to 30 days post-injection.

Please cite this article in press as: Laverne et al., Cholinergic interneuron inhibition potentiates corticostriatal transmission in direct medium spiny neurons and rescues motor learning in parkinsonism, Cell Reports (2022), https://doi.org/10.1016/j.celrep.2022.111034

In vivo electrophysiology

Mice were deeply anesthetized with a mixture of ketamine/xylazine (100/10 mg/kg, i.p. and supplemented as needed during the experiment) and mounted in a stereotaxic head frame (Horsley-Clarke apparatus; Unimécanique, Epinay-sur-Seine, France). Body temperature was maintained at 36.5°C with a homeothermic blanket controlled by a rectal probe (Harvard Apparatus, Holliston, MA). Extracellular recordings: single-unit activity of CINs was recorded extracellularly using glass micropipettes (25–35 MΩ) filled with a 0.5 M sodium chloride solution. Single neuron action potentials were recorded using the active bridge mode of an Axoclamp-2B amplifier (Molecular Devices, San Jose, CA), amplified, and filtered with an AC/DC amplifier (DAM 50; World Precision Instruments). CINs were identified by their classically defined electrophysiological characteristics: large spikes (width >2.5 ms) and ability to present tonic discharges (>1.0 Hz). Intracellular recordings: bipolar concentric stainless-steel electrode was inserted in the sensorimotor cortex (A: 2.0 mm; L: +1.5 mm; H: −0.6 mm from the cortical surface). Optical fiber (200 μm-diameter, 0.22 NA; Doric lenses, Québec, CA) was inserted in the striatum with a 15° angle and connected to a 100 mW laser (Combined dual wavelenght, DPSS laser system, Laserglow technologies, Toronto, Ontario, Canada). The entry point had the following coordinates: +0.7 mm AP, +2.6 mm ML. The fiber tip was at a depth of 1.5 mm from the cortical surface. Intracellular recordings of MSNs were performed while simultaneously recording the ECoG using a low-impedance (around 60 kΩ) silver electrode placed on the dura above contralateral motor cortex (+2.0 mm AP, −1.5 mm ML). This allows a precise on-line monitoring of the anesthesia level. Intracellular recordings were performed using 2 M K-acetate-filled glass microelectrodes (40–80 MΩ) and placed in the sensorimotor striatal region (+0.7 mm AP, +2.1 mm ML, −1.7/-2.7 mm DV) related to the stimulated cortical area. All recordings were obtained using an Axoclamp-2B amplifier (Molecular Devices, San Jose, CA) operated in the bridge mode. Data were sampled (300 Hz for ECoG and 25 kHz for intracellular recordings) and stored on-line on a computer connected to a CED interface using the Spike2 data acquisition software (Cambridge Electronic Design, Cambridge, UK). Impaled neurons were considered acceptable when their membrane potential was at least at −60 mV with spontaneous oscillations of large amplitude (>10 mV) and a spike amplitude >60 mV. Neurons that did not fill these criteria were discarded from the analysis. To measure the input resistance of MSNs, current pulses (200 ms duration applied at 0.5 Hz) were intracellularly injected through the recording electrode. As classically reported for MSNs recorded *in vivo* under ketamine/xylazine anesthesia (Mahon, 2001) the cells displayed slow membrane potential fluctuations consisting of recurrent sustained depolarizing plateaus interrupted by hyperpolarizing periods called down states. Cortically evoked EPSPs were induced by triggering the cortical stimulation during the down phase of the membrane potential oscillation detected with a window discriminator. Test stimulations (600-μs duration) in the sensorimotor cortex were applied at 0.1 Hz with an intensity below threshold for action potential induction. Two successive cortical stimulations were separated by a 10-s interval plus the time needed (few hundreds ms) for the next down state to occur and trigger the following cortical stimulation. In some cases, the down state was shorter than usual, triggering a cortical stimulation but with an EPSPs evoked after the end of the down state. Such EPSPs were not analyzed. The slope of the early part of the EPSPs was measured from the baseline to the first third of the peak response to estimate the mono-synaptic component of the EPSPs (Schulz et al., 2010), then averaged by bins of 100 s (n = 7–10 sweeps) and normalized. Induction of LTP at corticostriatal synapses: a cortical tetanization (100 Hz, 1-s duration repeated 4 times at 0.1 Hz) was delivered in conjunction with a 1-s post-synaptic depolarization achieved by intracellular injection of positive current (+1.0 nA). The intracellular injection of positive current induced a depolarization leading the membrane potential to a suprathreshold level for action potential firing. Current injection started 50 ms before and ended 50 ms after the cortical tetanus. For neurons in which the pairing protocol was combined with opto-inhibition of CINs, the light was switched on during the cortical tetanization, concomitantly to the post-synaptic depolarization. The synaptic responses recorded after the tetanus were normalized to pre-pairing values. Recordings were performed 19 to 27 days post-6-OHDA injection.

Immunohistochemistry

Immunohistochemical detection of TH and of GFP/mCherry was performed to control 6-OHDA lesion and eNpHR/DREADDs expression, respectively. To ensure the specificity of eNpHR or DREADDs expression in CINs, double immunohistochemical labeling of GFP/mCherry and ChAT was also performed as previously described (Maurice et al., 2015). Mice were deeply anesthetized with a mixture of ketamine/xylazine and then transcardially perfused with an ice-cold solution of paraformaldehyde 4% in PBS. After dissection, brains were post-fixed overnight in the same fixative at 4°C, cryoprotected in 30% sucrose dissolved in 1X PBS for an additional 36 h at 4°C, and frozen. Coronal cryostat sections (40 μm) covering the antero-posterior extent of the striatum or the SNc were used for labeling. For mice used in *in vitro* electrophysiology and FACS experiments, 250 μm fresh strital slices were fixed directly in 4% paraformaldehyde in PBS overnight. Brain sections were permeabilized in PBS with 0.4% Triton X-100 (PBST) for 30 min at room temperature. Sections were then incubated in a blocking solution composed of PBST with 5% bovine serum albumin for 1 h at room temperature. Free-floating sections were incubated overnight at 4°C in specific primary antibodies (mouse anti-TH 1/1000, Millipore, MAB318; rabbit anti-GFP 1/1000, Thermo Fisher Scientific, A11122; rabbit anti-RFP 2/1000, MBL International, PM005; goat anti-ChAT 1/100, Millipore, AB144P). After exposure to primary antibodies, two different protocols were used to reveal TH or GFP/Cherry/ChAT expression. For TH detection, sections were incubated in a PBS solution containing the biotinylated secondary antibody (goat anti-mouse horseradish peroxidase (HRP)-conjugated, 1/200, Jackson Immunoresearch, #115-065-166) for 1 h at room temperature. Immunoperoxidase detection was then performed by enzymatic reaction with an avidin-peroxidase complex for 1 h (Vectastain ABC HRP Kit Peroxidase Standard, Vector Lab.). After washing in PBS, the complex formed was revealed by incubation in 3,3′-Diaminobenzidine tetrahydrochloride (Sigmafast 3,3′-DAB tablets, D4293, Sigma-Aldrich). Following a final wash in PBS, slices

were mounted on superfrost slides and left to dry overnight. The next day, the slides were dehydrated and incubated in xylene baths, coverslipped and mounted in synthetic DPX mounting medium (Sigma Aldrich). Quantification of TH immunostaining was performed by digitized image analysis using "Densirag" analysis system (BIOCOM, France) in the striatum. For mice with intrastriatal injections (GIRK2 and rotarod experiments), quantification was performed at the SNc level. The mean optical density (OD) value was determined from at least two sections per animal after subtracting the background signal measured in a region lacking dopaminergic signal. The percentage of DA lesion was calculated from the ratio of OD measured in the 6-OHDA-injected side versus the corresponding non-injected side. To reveal GFP, mCherry and ChAT expression, sections were incubated in Alexa Fluor 488 and 555 donkey anti-rabbit (1/200, Thermo Fisher Scientific, A21206, A31572) and Alexa Fluor 594 donkey anti-goat (1/200, Thermo Fisher Scientific, A32758). Sections were then mounted onto SuperFrost Plus glass slides (VWR) and coverslipped with FluorSave mounting media (Merck Chemicals).

FACS-sorting

Striatal single cell suspensions were prepared after vehicle or 6-OHDA injection (28–31 days post-injection). 250 μm striatal slices were prepared as for *in vitro* electrophysiological recordings. Striata were then microdissected and incubated for 10 min in HibernateA minus calcium (Brainbits, HA-Ca) medium supplemented with 25 mM L-Glutamine (Gibco), pre-warmed at 37°C. Striatal pieces were then transferred to 10 mL sterilin tubes containing 3 mL of HA-Ca + 25 mM L-Glutamine medium supplemented with 2 mg/mL papaïn (Whortington) and 25 mg/mL dispase (Gibco) and incubated for 30 min at 37°C with shaking (200 rpm). After centrifugation for 5 min at 1100 rpm (room temperature), digestion medium was discarded and striatal pieces were transferred into 1 mL of ice-cold FACS-buffer containing HibernateA plus calcium, no phenol red (Brainbits), 2% (v/v) B27 supplement (Invitrogen) and 0.5 mM L-Glutamine (Gibco). Striatal pieces were mechanically triturated by realizing 7–10 passages through 22G, 23G and 26G needles. In between each type of needle, striatal pieces were allowed to settle for 2 min, 500 μL of suspension was filtered on a 70 μm cell strainer (Gibco), collected in a separate tube and maintained on ice. Then 500 μL of fresh FACS buffer were added to the striatal pieces before resuming the trituration. Finally, cells were precipitated by centrifugation for 20 min at 1100 rpm (4°C), medium was discarded and replaced with fresh ice-cold FACS buffer. Sytox Blue (ThermoFisher) viability dye was added to cells suspensions right before FACS. Tdtomato + MSNs were sorted on a FACS Aria cell sorter (BD Bioscience) by gating on Sytox Blue- (live cells) tdTomato + cells directly in ice-cold RLT lysis buffer from RNeasy Micro Kit (Quiagen), supplemented with 10% (v/v) β-mercaptoethanol (Sigma), and snap-frozen at −80°C before RNA extraction. During tissue preparation, 2 striatal slices per animal were spared to assess the extent of 6-OHDA lesion by anti-TH immunohistochemistry.

RNA extraction

RNA from sorted tdTtomato+ D1 MSNs was extracted using RNeasy Micro Kit (Quiagen), according to manufacturer's instructions. For quality and quantity determination, 1 μL of extracted RNAs was loaded on a Agilent Pico 6000 chip and ran on the 2,100 Bioanlayzer system (Agilent).

Reverse transcription followed by quantitative polymerase chain reaction (RT-qPCR)

2,2 ng of high-quality total RNA (RIN >8.5) were reverse-transcribed into cDNA using the Superscript III enzyme (ThermoFisher) and used as template for qPCR. Specific primers for the different genes of interest were designed using either the Universal ProbeLibrary (ProbeFinder version 2.5 for mouse, Roche Diagnostics) or PrimerBlast (NCBI) algorithm and chosen intron-spanning regions. Quantification of gene expression was done using Syber Green (ROX) master mix (Thermofisher) and the StepOne Real-Time PCR apparatus (ThermoFisher). Amplification of single PCR products was confirmed by the melting curves. The relative quantity of transcript encoding each gene vas determined by normalization to *Gapdh*, using the standard delta Ct method. The following primers were used:

- *Chrma1*-Fw: AAGATGGATTGAATGAGGCTGC, *Chrma1*-Rse: CCTCCAGTCACAAGATTTTTCTCA,
- *Chrma4*-Fw: CAGCGGAGCAAGACAGAAG, *Chrma4*-Rse: CATTGACAGGTGTGAAGTTCG,
- *Gapdh*-Fw: ATGGTGAAGGTCGGTGTGA, *Gapdh*-Rse: AATCTCCACTTTGCCACTGC.

Western blotting and quantification

Hemi-striata from non-lesioned or 6-OHDA mice were collected and immediately frozen in dry ice. The samples were homogenized at 4° in 200 μL of modified RIPA buffer (Tris-HCl 50 mM pH 8, NaCl 150 mM, NP40 1%, sodium deoxycholate 0.5%, SDS 0.1% with protease inhibitor cocktail). Homogenates were centrifuged at 10000 g for 10 min at 4 °C. Supernatants were aliquoted and stored at −80°C until use. Equivalent amounts of proteins present in each supernatant were denaturated with Laemmli buffer at 95°C for 5 min and were resolved by 10% SDS-PAGE and transferred onto nitrocellulose membranes (Biorad, 1620112). Blots were blocked by 5% milk for 1 h at 24°C and then immunoblotted with specific primary antibodies overnight at 4°C in blocking buffer. After incubation with species-specific secondary antibody linked to horseradish peroxidase (HRP), blots were detected using ECL western blot substrate (Millipore, WBKLS0500) and visualized with a BioRad imager. Primary antibodies used in these experiments included: mouse anti-TH (1/4000, Millipore, MAB318), rabbit anti-GIRK2 (1/500, Alomone labs, APC-006) and rabbit anti-GADPH (1/1000,

Abcam, Ab9485). The following goat HRP-conjugated secondary antibodies were used: anti-mouse (1/15000, Abcam, ab205719) and anti-rabbit (1/15000, Cell Signaling, 7074).

Rotarod

The apparatus (LE8205, Bioseb) consisted of a rod (30 mm in diameter) suspended horizontally at a height of 20 cm from the floor. Two days before starting the experiments, mice were placed for a few moments on the non-rotating cylinder to familiarize them with the experimental environment. Four trials per day were then performed for 5 days at constant speed (12 rpm) and the latency to fall from the rod was measured with a cut-off time of 60 s. Ten days after this training period, mice were tested for 3 days with accelerated speed, from 4 to 40 rpm over 300 s. Trials were spaced 15 min apart. Rotarod was performed 25 to 28 days after 6-OHDA and/or DREADD injections.

QUANTIFICATION AND STATISTICAL ANALYSIS

Data analysis was performed with Clampfit 10.7 (Molecular Devices, Inc.) and Spike 2 (Cambridge Electronic Design Limited, Cambridge, UK). The statistical analyses were two-tailed statistical tests with a risk α set at 0.05 and were performed in GraphPad Prism 9 software (San Diego, CA, USA). Within a set of experimental data, the paired t-test was used for dependent data except if the normality distribution test failed (Shapiro-Wilk test, $p < 0.05$). In the latter case, the Wilcoxon signed rank test was used. For independent data, we applied the normality (Shapiro-Wilk test) and equal variance tests. A t-test was used if the distributions were normal and the group variances were equal. Otherwise, the Mann-Whitney signed rank test was used. We used the 'nlme' package of R (R Core Team, 2013) to define a linear mixed-effects model (LME) of EPSP slopes (*in vivo* LTP data) and amplitudes (*in vitro* data). We used protocol and time as fixed effects together with a by-cell random slopes/amplitudes effects. Next, we used the R package 'emmeans' to perform the pairwise contrasts (Lenth et al., 2018) with adjusted p values for multiple testing using the Tukey procedure.

Cell Reports, Volume *40*

Supplemental information

Cholinergic interneuron inhibition potentiates corticostriatal transmission in direct medium spiny neurons and rescues motor learning in parkinsonism

Gwenaëlle Laverne, Jonathan Pesce, Ana Reynders, Etienne Combrisson, Eduardo Gascon, Christophe Melon, Lydia Kerkerian-Le Goff, Nicolas Maurice, and Corinne Beurrier

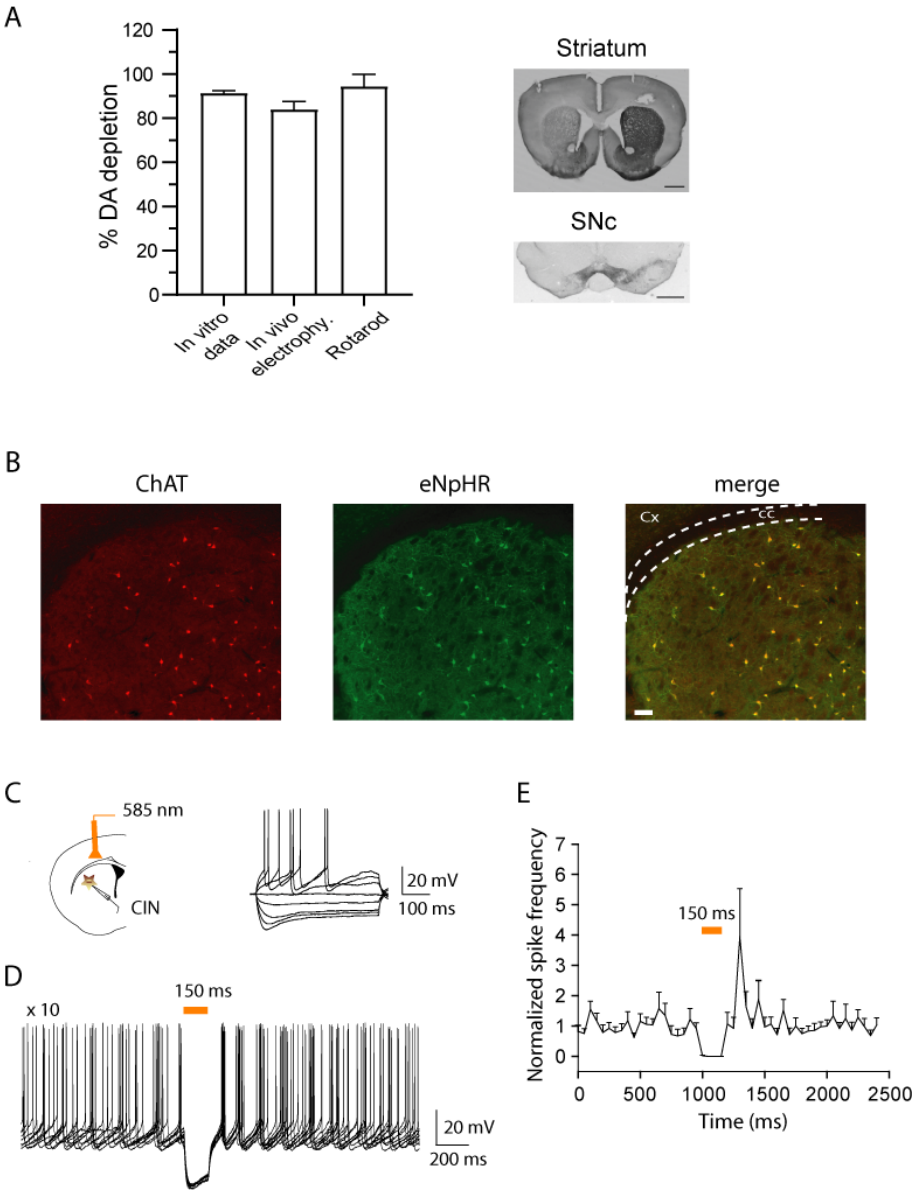

Figure S1: Assessement of the DA lesion extent and the efficacy of CIN opto-inhibition. Related to Figures 1, 2, 3, 4 and Supplemental Figures S2 and S4. (A) Percentage of DA depletion in 6-OHDA injected mice used in *in vitro* experiments (in vitro electrophysiology and FACS, n = 33), *in vivo* electrophysiological experiments (n=9) and rotarod experiments (n=19). TH immunostaining is performed in the striatum (n=37 mice) or SNc (n=24 mice). Scale bar: 1 mm. (B) Representative photomicrographs of striatal sections from a transgenic ChAT$^{cre/wt}$; Rosa$^{NpHr/wt}$ mouse showing ChAT (red) and eNpHR-EYFP (green)-expressing cells in the dorsal striatum. The merged image shows a total colocalization of ChAT+ and eNpHR+ cells. Cx: cortex, cc: corpus callosum. Scale bar: 100 µm. (C) Schematic of CIN activity recordings in slices from transgenic mice

expressing eNpHR in CINs. Membrane potential changes induced by current injection in one eNpHR-expressing CIN (-200 to +150 pA, 50 pA increment). (D) Current-clamp recording of the spontaneous firing of an individual CIN subjected to 150 ms light illumination repeated 10 times. (E) Normalized firing frequency (mean ± SEM) before, during and after 150 ms light application (n = 9). The spontaneous firing of eNpHR-expressing CINs is consistently inhibited by short-duration pulses of 585 nm light *in vitro.*

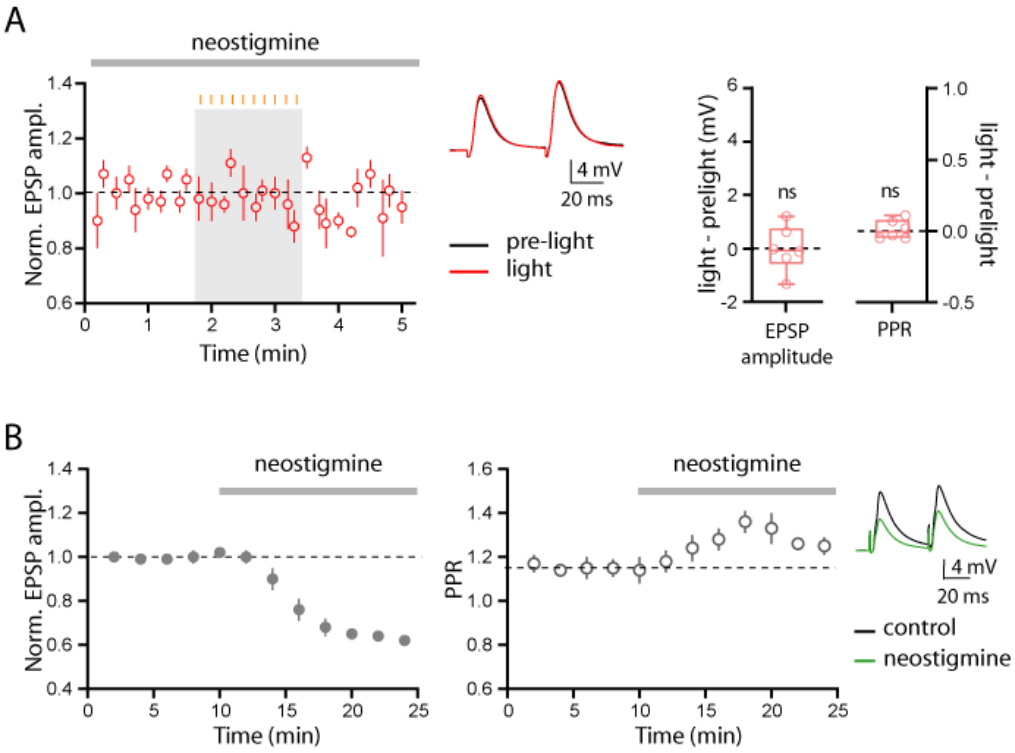

Figure S2: Increasing cholinergic tone does not reveal an effect of CIN opto-inhibition in non-lesioned mice. Related to Figure 1. (A) Time courses (mean ± SEM) of normalized EPSP amplitude in D1 MSNs (n = 6) before, during and after CIN opto-inhibition applied in the presence of neostigmine (3 µM). Light delivery (10 pulses, 150-ms width at 1 Hz) is indicated by the orange vertical bars above the grey rectangle. Representative example of averaged EPSP traces recorded before (pre-light) and during (light) opto-inhibition of CINs in the presence of neostigmine (3 µM). EPSPs are averages of ten consecutive trials. Box-and-whisker plots illustrate the difference in EPSP amplitude and PPR evoked in light vs. pre-light conditions and indicate median, first and third quartile, min and max values. (B) Time courses (mean ± SEM) of normalized EPSP amplitude and paired-pulse ratio in MSNs (n = 8 cells, N = 4 mice) showing the effect of neostigmine (3 µM, 15 min). Representative example of averaged EPSP traces (ten consecutive traces) before and after bath-application of neostigmine. ns, not significant. See Table S1 for statistical information.

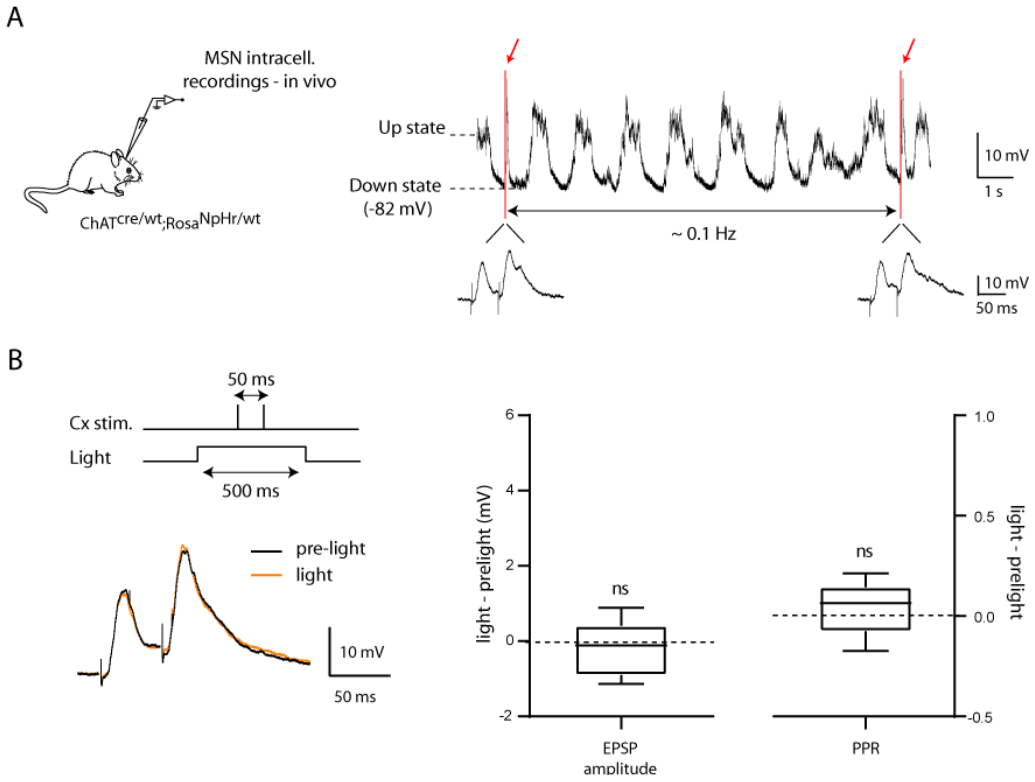

Figure S3: Corticostriatal transmission recorded *in vivo* in MSNs from non-lesioned mice is not affected by CIN opto-inhibition. Related to Figure 1. (A) Example of an intracellular recording from one MSN exhibiting up and down membrane fluctuations. Red arrows indicate the time when cortical stimulations were applied during the down states (paired stimulations at 50 ms interval). Expanded traces show the cortically-evoked EPSPs. (B) Representative example of averaged EPSP traces (8 consecutive trials) in MSNs recorded from non-lesioned mice before (pre-light) and during (light, 500-ms widht) opto-inhibition of CINs. The graphs illustrate the difference in EPSP amplitude and PPR evoked in light vs. pre-light conditions (n = 10). Box-and-whisker plots indicate median, first and third quartile, min and max values. ns, not significant. See Table S1 for statistical information.

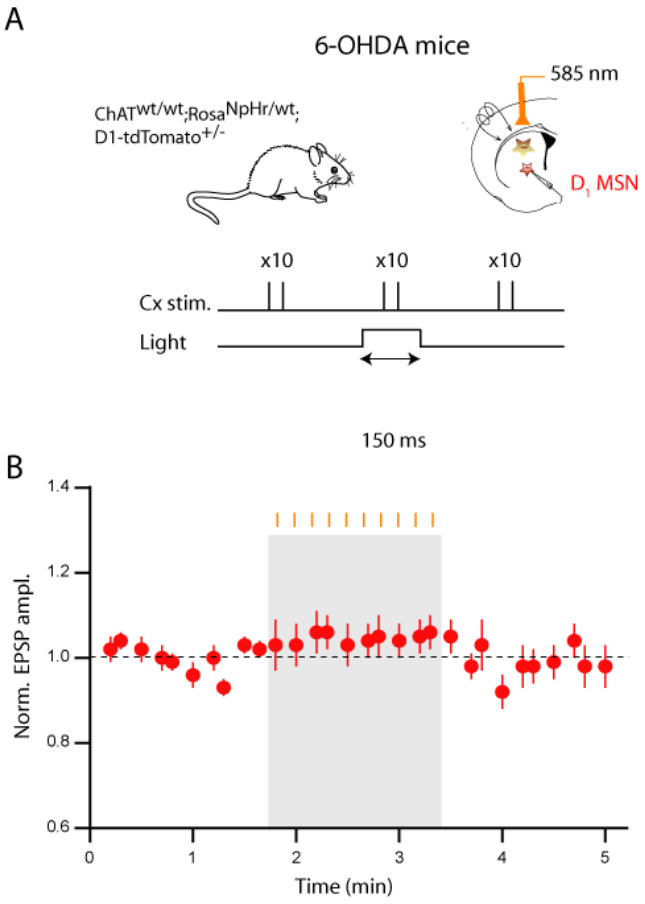

Figure S4: Light application does not modulate EPSPs in 6-OHDA mice that do not express eNpHR. Related to Figure 1. (A) Schematic of experimental protocol. Mice do not express Cre recombinase in cholinergic neurons. (B) Time courses (mean ± SEM) of normalized EPSP amplitude recorded in 6-OHDA mice (n = 18) before, during and after CIN opto-inhibition. Light delivery (10 pulses, 150-ms widht at 1 Hz) is indicated by the orange vertical bars above the grey rectangle. See Table S1 for statistical information.

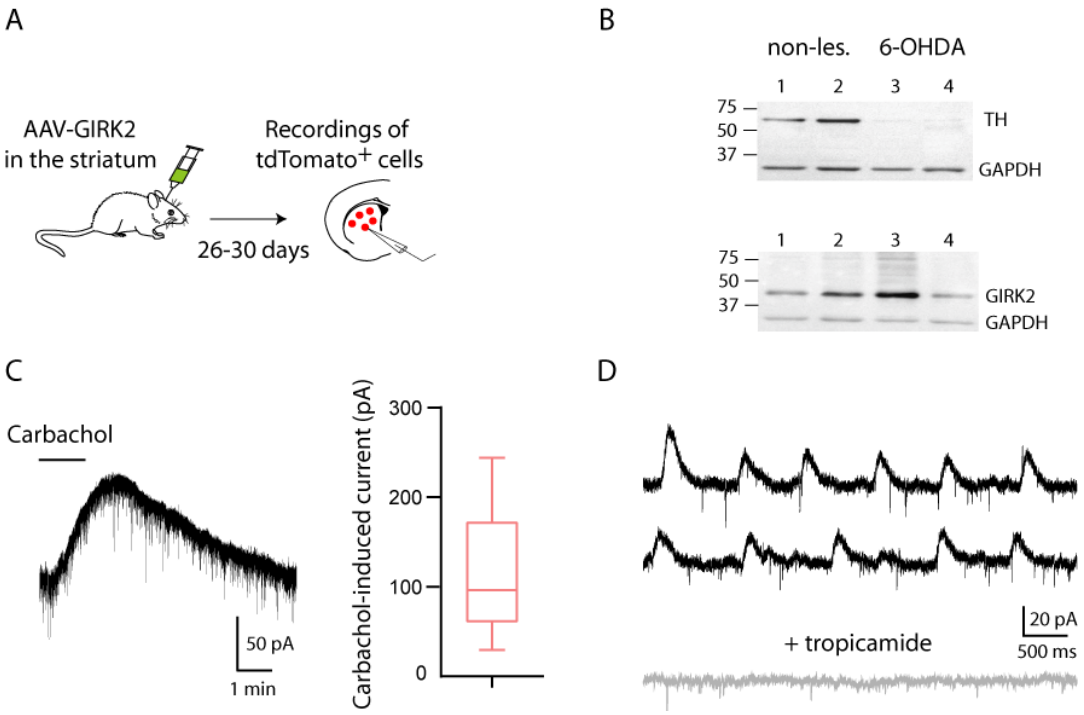

Figure S5: GIRK2 channels couple efficiently to Gαi-linked M4 mAChR. Related to Figure 2. (A) Schematic of the experimental approach. (B) Immunoblot images of GIRK2 expression in non-lesioned (n = 2) and 6-OHDA (n = 2) mice. (C) Bath-application of the muscarinic agonist carbachol (10 µM, 2 min) evoked an outward current in a tdTomato+ MSN recorded in voltage-clamp mode (Vh = -70 mV). Box-and-whisker plot shows the amplitude of the carbachol-induced currents in tdTomato+ cells (n = 5). (D) Representative traces illustrating the blockade of sIPSCs recorded in a tdTomato+ MSN (Vh = -60 mV) by the preferential antagonist of M4 mAChR, tropicamide (1 µM).

SUPPLEMENTAL TABLES

Table S1. Related to Figures 1, 2, S2, S3 and S4

Figure		Parameter	n (neurons/mice)	Condition	Median	Interquartile range		Statistical test	p value
						25 %	75 %		
Fig. 1	1B	EPSP ampl. (mV) D1 MSNs non-les. mice	12 / 8	Pre-light	12.73	9.78	15.82	Wilcoxon signed rank test	p = 0.1821
				Light	13.53	10.71	15.64		
		PPR D1 MSNs non-les. mice	12 / 8	Pre-light	1.245	1.116	1.435	Wilcoxon signed rank test	P = 0.4570
				Light	1.290	1.098	1.378		
	1C	EPSP ampl. (mV) D1 MSNs 6-OHDA mice	13 / 9	Pre-light	12.55	9.56	15.16	Wilcoxon signed rank test	p = 0.0024
				Light	13.64	11.68	15.99		
		PPR D1 MSNs 6-OHDA mice	13 / 9	Pre-light	1.33	1.28	1.48	Wilcoxon signed rank test	p = 0.8652
				Light	1.33	1.22	1.50		
	Between-group comparison	**Parameter**	**n (neurons/mice)**	**Effect size ± SEM**		**Degree of Freedom**		**Confidence interval**	**p value**
	1B, C	EPSP ampl. (mV) D1 MSNs non-les. vs 6-OHDA	Non-les.: 12 / 8 6-OHDA: 13 / 9	-0.234 ± 0.0902		12		[-0.4306, -0.0374]	p = 0.0096 ¤
	¤ After obtaining the most optimal LME model, pairwise comparisons of the EPSP amplitudes were performed with 95% confidence interval and p-values adjusted for multiple testing using the Tukey's procedure.								

Figure		Parameter	n (neurons/mice)	Condition	Median	Interquartile range		Statistical test	p value
						25 %	75 %		
Fig. S2	S2A	EPSP ampl. (mV) D1 MSNs non-les. mice + neostigmine	6 / 5	Pre-light	8.12	5.93	11.70	Paired t-test	p = 0.9893
				Light	8.23	5.14	12.57		
		PPR D1 MSNs non-les. mice + neostigmine	6 / 5	Pre-light	1.295	1.160	1.353	Paired t-test	p = 0.6838
				Light	1.280	1.203	1.400		
Fig. S3	S3B	EPSP ampl. (mV) MSNs non-les. mice / in vivo	10 / 6	Pre-light	10.47	6.05	13.63	Wilcoxon signed rank test	p = 0.5566
				Light	9.77	6.30	12.95		
		PPR MSNs non-les. mice / in vivo	10 / 6	Pre-light	1.770	1.503	2.556	Wilcoxon signed rank test	p = 0.3750
				Light	1.692	1.595	2.657		
Fig. S4	S4	EPSP ampl. (mV) D1 MSNs 6-OHDA mice / no opsin	18 / 5	Pre-light	12.05	9.10	14.83	Wilcoxon signed rank test	p = 0.2381
				Light	11.45	9.18	17.13		
		PPR D1 MSNs 6-OHDA mice / no opsin	18 / 5	Pre-light	1.250	1.000	1.400	Wilcoxon signed rank test	p = 0.1558
				Light	1.300	1.100	1.500		

Fig. 2	2D	EPSP ampl. (mV) D1 MSNs 6-OHDA mice + tropicamide	10 / 2	Pre-light	13.11	10.54	14.95	Wilcoxon signed rank test	p = 0.3223
				Light	13.68	10.55	15.66		
		PPR D1 MSNs 6-OHDA mice + tropicamide	10 / 2	Pre-light	1.385	1.235	1.620	Wilcoxon signed rank test	p = 0.0820
				Light	1.355	1.205	1.563		
	2D	EPSP ampl. (mV) D1 MSNs 6-OHDA mice + PKI pipette	10 / 2	Pre-light	8.77	5.38	14.41	Wilcoxon signed rank test	p = 0.4961
				Light	9.41	5.83	14.02		
		PPR D1 MSNs 6-OHDA mice + PKI pipette	10 / 2	Pre-light	1.130	1.115	1.273	Wilcoxon signed rank test	p = 0.2324
				Light	1.160	1.040	1.213		
	2E	qPCR: relative expression *Chrma1* (arbitrary unit)	na / 7	Non-les. mice	0.02054	0.01873	0.02256	Mann-Whitney signed rank test	p = 0.5350
			na / 7	6-OHDA mice	0.02193	0.02100	0.02240		
		qPCR: relative expression *Chrma4* (arbitrary unit)	na / 7	Non-les. mice	0.02335	0.02051	0.02509	Mann-Whitney signed rank test	p = 0.1649
			na / 7	6-OHDA mice	0.03044	0.02152	0.03247		
	2F	sIPSC frequency (Hz)	7 / 2	Non-les. mice	1.72	1.50	1.92	Unpaired t-test	p = 0.1005
			10 / 5	6-OHDA mice	1.28	1.03	1.52		
		sIPSC amplitude (pA)	7 / 2	Non-les. mice	27.95	19.40	46.69	Mann-Whitney signed rank test	p = 0.2698
			10 / 5	6-OHDA mice	21.72	17.48	28.16		

Table S2. Related to Figures 3 and 4

Figure		Parameter	n (neurons/mice)	Condition	Mean ± SEM	Statistical test	p value
Fig. 3	3C	EPSP slope (mV/ms) non-les. mice - Average	6 / 6	Pre-pairing	11.80 ± 0.66	Two-tailed Paired t test	p = 0.0036
				Post-pairing (20-30 min)	15.45 ± 0.72		
	3C	EPSP slope (mV/ms) 6-OHDA mice - Average	5 / 4	Pre-pairing	8.25 ± 0.14	Two-tailed Paired t test	p = 0.2076
				Post-pairing (20-30 min)	8.64 ± 0.14		
	3C	EPSP slope (mV/ms) 6-OHDA mice + CIN inhib. - Average	5 / 5	Pre-pairing	7.88 ± 0.24	Two-tailed Paired t test	p = 0.0010
				Post-pairing (20-30 min)	9.62 ± 0.08		
	Between-group comparison	**Parameter**	**n (neurons/mice)**	**Effect size ± SEM**	**Degree of Freedom**	**Confidence interval**	**p value**
	3D	EPSP slope (mV/ms) non-les. vs 6-OHDA	Non-les.: 6 / 6 6-OHDA: 5 / 4	3.5389 ± 1.1664	13	[1.019, 6.0587]	p = 0.0061 ¤
	3D	EPSP slope (mV/ms) non-les. vs 6-OHDA + CIN inhib.	Non-les.: 6 / 6 6-OHDA + CIN inhib.: 5 / 5	1.8012 ± 1.0013	13	[-0.362, 3.9643]	p = 0.1717 ¤
	3D	EPSP slope (mV/ms) 6-OHDA vs 6-OHDA + CIN inhib.	6-OHDA: 5 / 4 6-OHDA + CIN inhib.: 5 / 5	-1.7377 ± 1.033	13	[-3.9694, 0.4939]	p = 0.2139 ¤
	¤ After obtaining the most optimal LME model, pairwise comparisons of the EPSP slopes were performed with 95% confidence interval and p-values adjusted for multiple testing using the Tukey's procedure.						

Figure		Parameter	n (neurons/mice)	Condition	Mean ± SEM	Statistical test	p value
Fig. 4	4D	Latency to fall (sec) non-les. + mCherry	na / 9	Day 1	107.20 ± 8.83	Wilcoxon signed rank test	p = 0.0039
				Day 3	157.90 ± 9.60		
		Latency to fall (sec) 6-OHDA + hM4Di-mCherry	na / 7	Day 1	89.49 ± 14.29	Wilcoxon signed rank test	p = 0.0313
				Day 3	132.90 ± 19.15		
		Latency to fall (sec) 6-OHDA + mCherry	na / 12	Day 1	81.03 ± 8.85	Wilcoxon signed rank test	p = 0.5186
				Day 3	95.23 ± 11.95		